


Article

Numerical Investigation on the Influence of Injection Location and Injection Strategy on a High-Pressure Direct Injection Diesel/Methanol Dual-Fuel Engine

Huabing Wen ^{1,*}, Yue Yu ¹, Jingrui Li ¹, Changchun Xu ¹ , Haiguo Jing ² and Jianhua Shen ²

¹ School of Energy and Power, Jiangsu University of Science and Technology, Zhenjiang 212114, China; 211110803112@stu.just.edu.cn (Y.Y.)

² CSSC Marine Power Co., Ltd., Zhenjiang 212002, China

* Correspondence: whb@just.edu.cn; Tel.: +86-139-5289-4094

Abstract: High-pressure direct injection diesel/methanol dual-fuel engines exhibit excellent emission reduction potential, but they are still in the initial stage of research and development. The influences of different methanol injection locations, injection duration, and injection pressures on combustion characteristics, mixture homogeneity, and exhaust emissions are investigated to explore appropriate injection strategies and further optimize the engine performance base using CONVERGE software. The results show that the impact of the methanol injection position on the engine is relatively small, especially on combustion characteristics. A larger axial nozzle distance contributes to the formation of the homogeneous mixture, improving the engine economy. However, the engine performance is remarkably affected by methanol injection duration and methanol injection pressure. A shorter combustion duration is achieved with a decrease in the methanol injection duration and an increase in the methanol injection pressure, as a result of which the fuel economy is improved, with the combustion process more concentrated near the top dead center. Simultaneously, the mixture homogeneity is enhanced, which is conducive to a reduction in soot and CO emissions, yet not to a NO_x and HC reduction. The lowest overall emissions of NO_x, soot, CO, and HC are achieved when the radial nozzle distance and axial nozzle distance are 2.5 mm and 0.5 mm, respectively. Besides, the combustion characteristics and emissions of the engine are affected significantly under different methanol injection locations and injection pressures. The increased injection interval leads to deteriorating combustion characteristics and economy, i.e., a delayed combustion phase (CA₅₀), an extended ignition delay and combustion duration (CA₁₀–CA₉₀), thereby increasing CO and soot emissions, but decreasing NO_x emission. Additionally, the optimal economy and exhaust emissions are obtained when adopting an injection duration of 6 °CA and an injection pressure of 44.4 MPa. The ITE is increased in this case compared to the other injection strategies, thereby improving the engine performance significantly. The results provide parametric feedback and theoretical support for the design of high-pressure direct injection diesel/methanol dual-fuel engines from a time and space perspective, which has certain theoretical significance.

Keywords: methanol; high-pressure direct injection; injection strategy; engine performance; exhaust emissions



Citation: Wen, H.; Yu, Y.; Li, J.; Xu, C.; Jing, H.; Shen, J. Numerical Investigation on the Influence of Injection Location and Injection Strategy on a High-Pressure Direct Injection Diesel/Methanol Dual-Fuel Engine. *Energies* **2023**, *16*, 4518. <https://doi.org/10.3390/en16114518>

Academic Editors: Roberto Finesso and Massimo Cardone

Received: 27 April 2023

Revised: 17 May 2023

Accepted: 2 June 2023

Published: 4 June 2023



Copyright: © 2023 by the authors. Licensee MDPI, Basel, Switzerland. This article is an open access article distributed under the terms and conditions of the Creative Commons Attribution (CC BY) license (<https://creativecommons.org/licenses/by/4.0/>).

1. Introduction

On account of the adverse effects of the global warming phenomenon and the growing problem of environmental pollution, governments around the globe are being forced to implement increasingly stringent emission regulations. The exhaust emissions of engines have long been identified as a major source of pollutants [1,2], as a result of which they bear the brunt of reducing emissions, particularly carbon emissions. Currently, the search for clean alternative fuels and advanced injection strategies has become the key for engines to break through existing technological barriers [3–6]. Methanol is a low-carbon alternative fuel

with a low hydrocarbon ratio, rich oxygen content, and a high latent heat of vaporization, showing good application prospects in emission reduction [7–10].

The main operating modes of methanol in engines include direct mixing [1,11–13], port injection, and in-cylinder direct injection [14]. Expensive additives are required for the direct mixing method, thereby increasing the operating cost [15]. A small amount of diesel is injected to ignite the methanol injected directly into the intake port using the port injection method [16], which has attracted extensive attention [17,18]. Yao et al. [19,20] proposed the concept of a diesel methanol compound combustion system, and experimentally investigated its influence on engine performance, revealing that the port injection method led to a better economy, lower NO_x and soot emissions, and higher CO and HC emissions. Xu et al. [21] experimentally studied the influence of the methanol substitution rate (MSR) on engine emissions under different loads. MSR is defined as the proportion of the calorific value released by methanol to the total fuel calorific value in this study. It was found that NO_x emission decreased, whereas increased CO and HC emissions were caused by the increase in MSR. It is obvious that the trade-off relationship between NO_x and HC fails to be balanced by the port injection method in a high MSR. Therefore, research on the in-cylinder direct injection method needs to be conducted to reduce exhaust emissions.

The in-cylinder direct injection method achieves high-pressure direct injection of diesel and methanol in the cylinder, with a small amount of diesel serving as an ignitor [22]. Wang et al. [23] carried out a study on the combustion characteristics of ignition diesel and in-cylinder directly injected methanol, based on a constant volume chamber. The results showed that incomplete combustion of methanol existed in some areas, resulting in increased HC emission. The inhomogeneous methanol mixture had almost no inhibitory effect on combustion when diesel was injected at low pressure, while it achieved the opposite at high pressure. Ning et al. [24] carried out experimental research on the combustion characteristics of engines fueled with directly injected methanol under various MSR and methanol injection timings (M_{SOI}). Jia et al. [25] explored the influence of MSR and methanol injection pressure on direct injection diesel/methanol dual-fuel engines. The results indicated that methanol injection pressure had a certain impact on the combustion process of the diesel/methanol direct injection engine, thereby reducing the carbon emissions at each load. Therefore, the injection strategies for direct injection of methanol have great investigation value.

Recently, due to the technical difficulties of cylinder head modification and the complexity of fuel injector structure, a few studies have mainly focused on the numerical simulation of injection strategies, and the MSR has been investigated with a direct injection diesel/methanol dual-fuel engine [14,26–28]. When controlling variables, different methanol injection durations correspond to different injection pressures. As a key structural parameter of the coaxial injector, the injection location plays an important role in improving the mixture homogeneity, thus affecting the combustion and emissions [29]. Besides, it is extremely important to select the injection location reasonably, in view of the high vaporization latent heat of methanol. Because the distance between methanol spray and pilot diesel will make an impact on ignition temperature, which is related to the combustion stability of the engine, it may thus lead to incomplete combustion and increased exhaust emissions [30]. Therefore, it is very important to investigate the effect of the injection location and injection strategies on the combustion process, and to select the optimal combination of injection location and injection strategies.

In order to reveal the relationship between methanol injection strategies and engine performance, and explore the appropriate methanol injection location and injection strategies for high-pressure direct injection diesel/methanol dual-fuel engines, the numerical simulation method is adopted to study the effects of methanol injection location, methanol injection duration, and methanol injection pressure on the combustion, mixture homogeneity, and exhaust emissions of a direct injection diesel/methanol dual-fuel engine under three different injection intervals. The investigation of methanol injection strategies is based on the optimal injection location. Many studies have been conducted to investigate the

influence of fuel injection strategies (including injection timing and injection pressure) on the performance of the methanol port-injection engine. However, unlike the port-injection engine, the in-cylinder direct injection diesel/methanol engine involves the matching of the directly injected methanol spray, diesel spray, and air. This matching process is more complex than the previous engines, which could affect the mixing homogeneity and the engine performance, causing the direct injection diesel/methanol dual-fuel engine to stay in the early stages of development. Therefore, investigation of the influence of the injection strategies is valuable in this kind of engine. Additionally, the influence of the methanol injection location on the performance of direct injection diesel/methanol dual-fuel engines is rarely studied. Therefore, this study provides theoretical support and parametric feedback for the development and design of high-pressure direct injection diesel/methanol dual-fuel engines from a time and space perspective innovatively, which has certain theoretical value.

2. Model Establishment and Calibration

The high-pressure direct injection diesel/methanol dual-fuel engine is modified base on a four-cylinder turbocharged and intercooled diesel engine with the specifications shown in Table 1. The 3-D computational fluid dynamics (CFD) model of the cylinder chamber is established using CONVERGE 3.0 software. The mesh of the chamber in TDC is displayed in Figure 1. The general properties of diesel and methanol are listed in Table 2. The crank angles for the simulation start from the intake valve close (IVC) to the exhaust valve open (EVO). For the convenience of understanding the output results, 0 °CA is selected as TDC of the compression stroke. The initial temperature and pressure in the cylinder is 377 K and 1.92 bar. The initial gas in the cylinder is air, without considering the influence of exhaust gas. The boundary of the cylinder head and the cylinder wall are stationary, but the piston is in motion. The temperature of the cylinder head, cylinder wall, and piston boundary is 520 K, 420 K, and, 590 K, respectively. The message-passing interface is used to run the calculation in parallel to improve the computational efficiency.

Table 1. Main specifications of the engine.

Items	Values
Bore × Stroke	108 × 115 mm
Compression ratio	16.5
Displacement	4.214 L
Rated speed	1660 r/min
IVC	−130 °CA ATDC
EVO	112 °CA ATDC
Methanol nozzle (number/diameter)	7/0.42 mm
Diesel nozzle (number/diameter)	7/0.18 mm
Combustion chamber	ω type

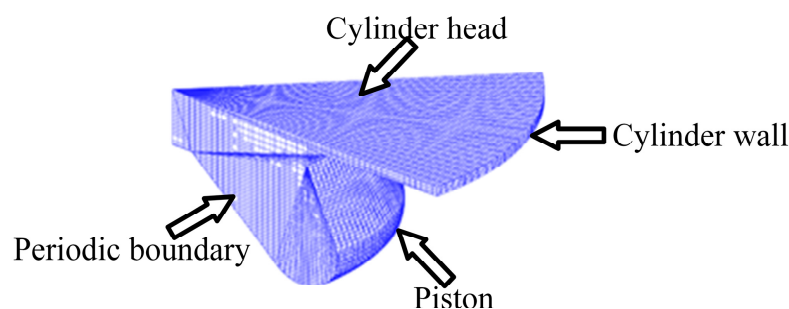


Figure 1. Diagram of mesh in TDC.

Table 2. Properties of diesel and methanol [31].

Fuel Properties	Diesel	Methanol
Formula	$C_{12}H_{26}-C_{14}H_{30}$	CH_3OH
Density (kg/m^3 , @ 20 °C)	840	795
Viscosity (mPa s @ 298.15 K)	3.35	0.59
Auto-ignition temperature (°C)	260	470
Latent heat (kJ/kg)	270	1109
Lower heating value (MJ/kg)	42.5	19.7
Cetane number	40–55	3
Laminar flame speed (m/s)	0.39	0.523
Oxygen content (% mass)	0	50

2.1. Governing Equations

The engine in-cylinder working process involves complex physical and chemical processes such as flow, spray, and combustion, but these processes all follow the conservation equations of mass, momentum, and energy.

The mass conservation equation for compressible fluids is given by

$$\frac{\partial \rho}{\partial t} + \frac{\partial \rho u_i}{\partial x_i} = S \quad (1)$$

where ρ is density, u is velocity, and S is the source item.

The momentum conservation equation for compressible fluids is given by

$$\frac{\partial \rho u_i}{\partial t} + \frac{\partial \rho u_i u_j}{\partial x_j} = -\frac{\partial P}{\partial x_i} + \frac{\partial \sigma_{ij}}{\partial x_j} + S_i \quad (2)$$

where P is the pressure, and σ_{ij} is the viscous stress tensor.

The energy conservation equation for compressible fluids is expressed as follows:

$$\frac{\partial \rho e}{\partial t} + \frac{\partial \rho e u_j}{\partial x_j} = -P \frac{\partial u_j}{\partial x_j} + \frac{\partial u_i}{\partial x_j} \delta_{ij} + \frac{\partial}{\partial x_i} \left(K \frac{\partial T}{\partial x_i} \right) + \frac{\partial}{\partial x_j} \left(\rho D \sum_m h_m \frac{\partial \gamma_m}{\partial x_j} \right) + S_i \quad (3)$$

where m represents a certain species, e is the specific internal energy, K is the thermal conductivity, T is the temperature, D is the mass diffusion coefficient, h_m is the enthalpy of the substance, and γ_m is the mass fraction of the species m .

The pressure implicit in the splitting of operator (PISO) method, which is based on the finite difference method and the finite volume method, is used by CONVERGE to numerically solve the conservation equations. Convergence tolerances of 1×10^{-5} , 1×10^{-8} , 1×10^{-4} , and 1×10^{-4} and maximum iterations of 50, 500, 2, and 2 are set for momentum, pressure, density, and energy, respectively. Once the residual value is equal to or lower than the specified convergence tolerance, the solution is considered convergent. In addition, the initial time-step, minimum time-step, and maximum time-step are set as 1×10^{-7} , 1×10^{-8} , and 1×10^{-4} s, respectively.

2.2. Selection of Sub-Models

CONVERGE software contains numerous physical models. The combustion in a cylinder involves complex physical processes such as the breakup and atomization of the spray, the chemical reaction of fuel, heat and mass transfer, and the flow of air, etc. Therefore, the accuracy of the simulation can be improved by selecting a reasonable model base on the actual working conditions of the engine. The chemical reaction mechanism is the diesel/methanol dual-fuel skeletal mechanism sourced from the results of Jia [32], which consists of 53 components and 176 reactions. The physical sub-models adopted in the research are listed in Table 3.

Table 3. Sub-models in use.

Description	Sub-Models
Turbulence	RNG κ - ϵ model [33]
Spray collision	Wall film [34]
Droplet breakup	KH-RT [35]
Wall heat transfer	Han and Reitz [36]
Droplet collision	NTC [37]
Combustion	SAGE [38]
NO _x formation	Extended Zeldovich model [39]
Soot formation	Hiroyasu soot model [40]

2.3. Simplified Model Establishment

A coaxial diesel/methanol dual-fuel injector with seven nozzles is arranged in the center of the cylinder head, the modification of which is simplified. The injector can control the amount of fuel injected while ensuring satisfactory mixture homogeneity, which is conducive to giving full play to the ignition performance of micro-pilot diesel and achieving a high MSR. A 1/7 simplified model of the chamber is established to save simulation time, according to the symmetry of the injector nozzles. Meanwhile, the in-cylinder pressure and heat release rate (HRR) are compared and analyzed to verify the calculation accuracy, based on the full-cylinder model and the simplified model shown in Figure 2c.

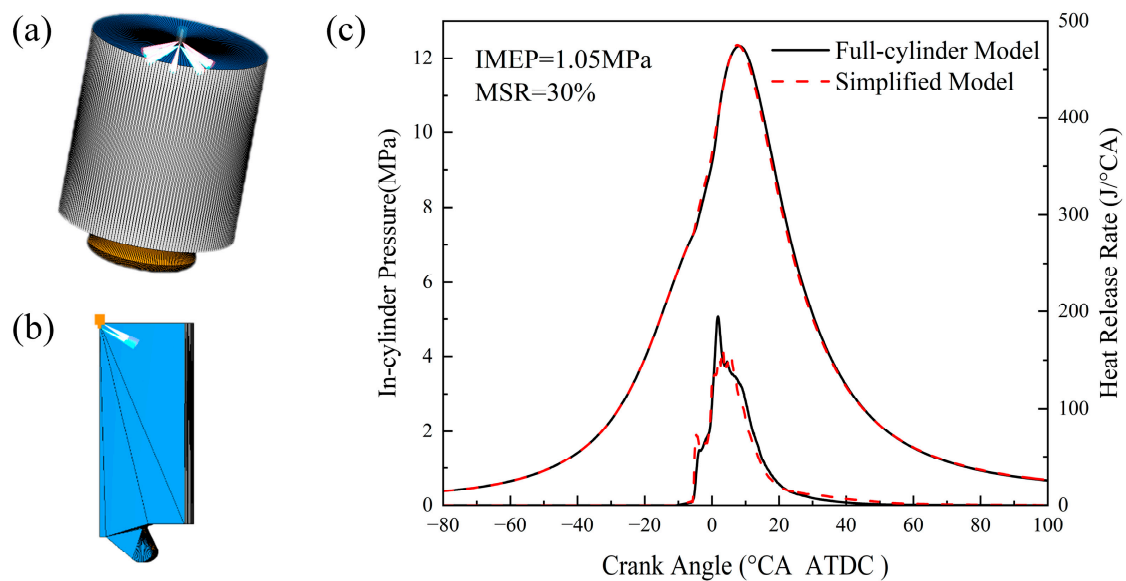


Figure 2. Establishment of the simplified model. (a) Full-cylinder model in BDC. (b) 1/7 simplified model in BDC. (c) Calibration of the simplified model.

The calibration results of the simplified model are depicted in Figure 2c. As observed from Figure 2c, the in-cylinder pressure of the simplified model and the full-cylinder model are in good agreement. A slight error in HRR is observed at the peak. The neglect of the spray interaction in the simplified model, which slows down the HRR, accounts for the difference. However, compared with the full-cylinder model, the variation trend in HRR is the same in the simplified model with high prediction accuracy and reliability; thus, the simplified model can be used for the following research.

2.4. Grid Independence Analysis

The grid independence analysis is implemented on account of the complex physical and chemical processes coupled in the chamber. The base grid size is set to 3 mm, 3.5 mm, 4 mm, 4.5 mm, and 5 mm. The adaptive mesh refinement (AMR) is adopted to refine the

grids wherein the variation of temperature and speed exceeded 5 K and 2 m/s. Simultaneously, the fixed embedding of 3 levels is set, respectively for the spray, piston, and cylinder wall. The influences of different base grids on the in-cylinder pressure are displayed in Figure 3a. The in-cylinder pressure of five base grids agrees well, with slight error at the peak. The in-cylinder pressure error corresponding to the 4 mm base grid is less than 2.7%, and the calculation time is only 50% of the 3 mm grid. Figure 3b shows that the AMR embedding level has less influence on the calculation. Considering the simulation accuracy and time cost, the 4 mm grid is chosen as the basic grid, with a maximum AMR embedding level of 3 for subsequent research, which leads to a minimum base grid of 0.5 mm during the simulation calculation.

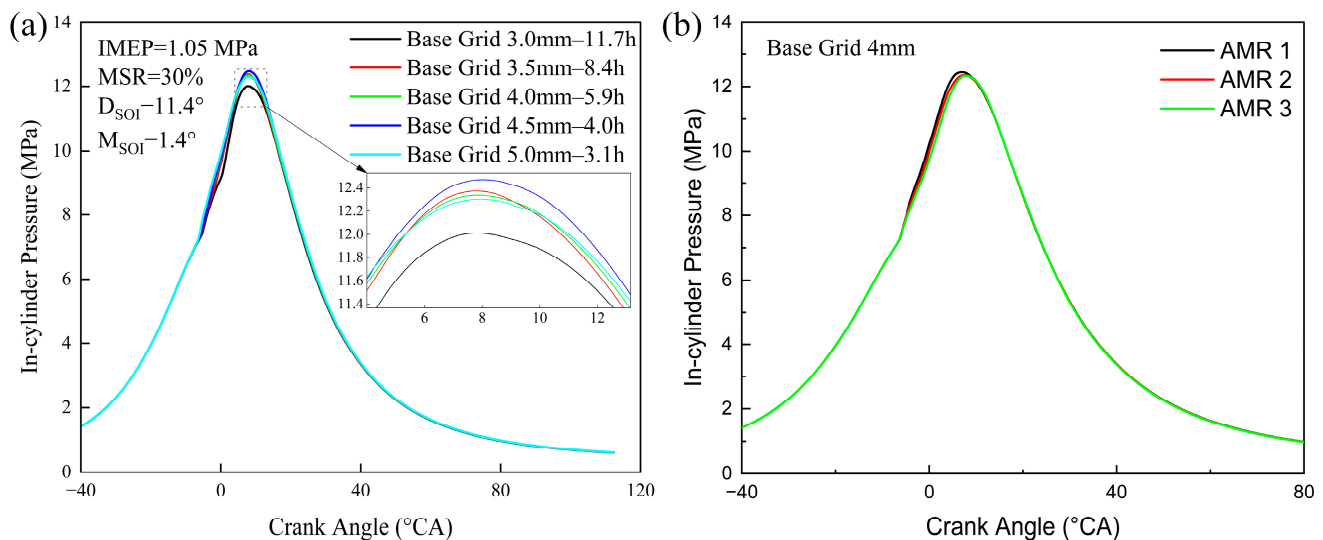


Figure 3. Grid independence study. (a) Base grid; (b) AMR grid.

2.5. Calibration of 3-D CFD Model

To ensure the reliability of the calculation results, the simulation model established above is calibrated using the test data of methanol port injection in this section [14]. The calibration test data are sourced from Zang [41]. The in-cylinder pressure and HRR under different conditions are compared in detail, as well as the emissions of NO_x and soot. The parameter settings for the calibration are listed in Table 4.

Table 4. Operation conditions of calibration.

Parameters	Condition 1	Condition 2	Condition 3	Condition 4
Engine load (%)	25	75	75	75
MSR (%)	0	0	30	40
Engine speed (r/min)	1660	1660	1660	1660
M_{SOI} (°CA ATDC)	-	-	-1.4	-1.4
Initial pressure (MPa)	0.157	0.2	0.196	0.194
Initial temperature (K)	372	385	379	378

The simulated in-cylinder pressure curve agrees well with the test results, as can be seen from Figures 4 and 5. Due to the use of dual Y-axis curves, in Figures 4 and 5, the direction indicated by the black arrow represents the Y-axis corresponding to the curve. There is only a slight error in the numerical value of HRR, which is caused by the difference in the specific heat ratio [42] and the atomization effect between the direct injection method and the port injection method. Besides, the exhaust emission curve is completely consistent with the changing trend in the experimental results. Therefore, the simulation model is believed to have high reliability, referring to relevant literature [43,44].

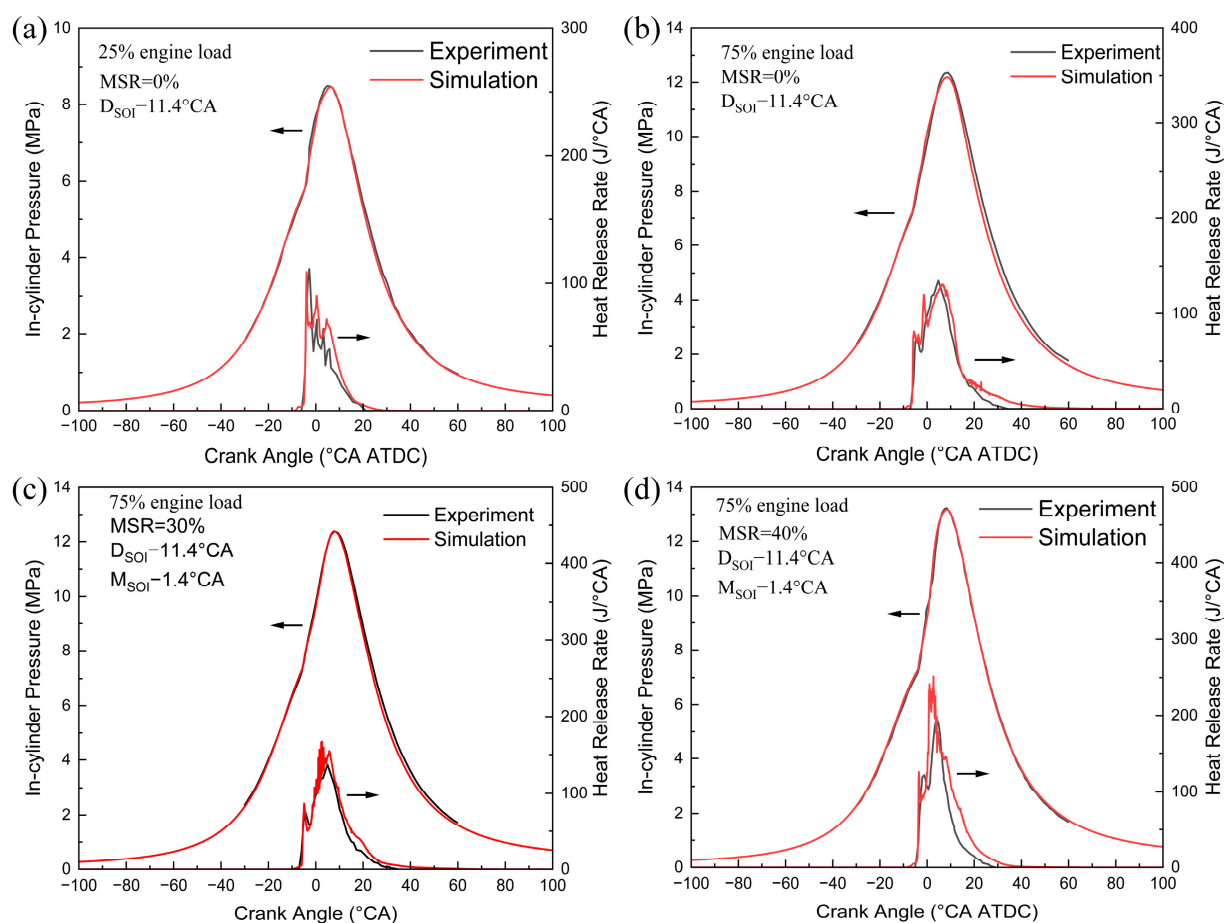


Figure 4. Calibrations of in-cylinder pressure and HRR: (a) condition 1; (b) condition 2; (c) condition 3; (d) condition 4.

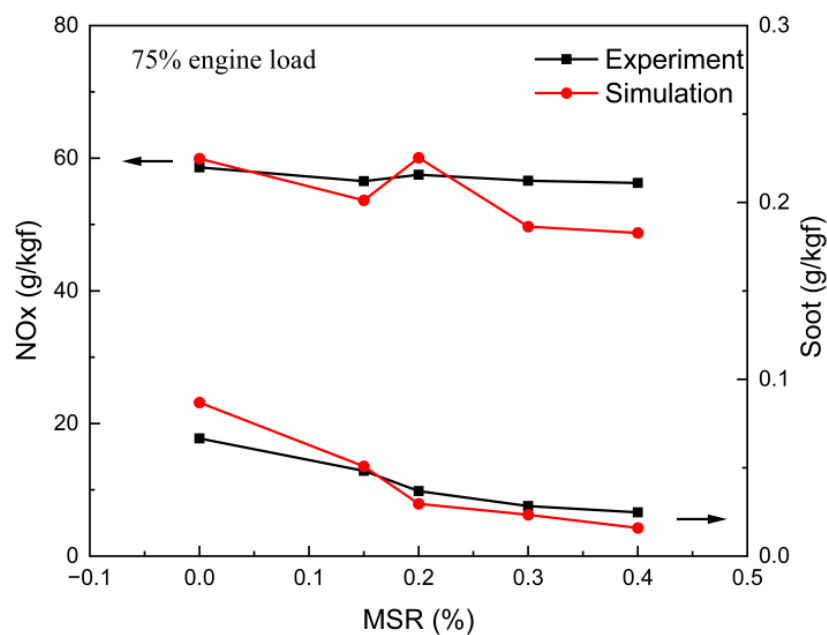


Figure 5. Calibration results for NO_x and soot emissions.

3. Results and Discussion

In the study, only the 75% load (IMEP \approx 1.05 MPa) condition with a constant engine speed at 1660 r/min is selected for the study, in view of the fact that the engines normally operate at 75% load. N-heptane, which has similar combustion characteristics to diesel, is selected as the characteristic fuel of diesel. The injection duration and injection pressure of the micro-pilot diesel are fixed at 6 °CA and 50 MPa, respectively. MSR has a notable influence on engine performance, and a higher MSR can reduce carbon emissions effectively [26]. Therefore, the fixed MSR (by energy) is 95%, and the total fuel calorific value (E_{fuel}) of the methanol and micro-pilot diesel per cycle is 2506 J. In this study, the calculation formulas for E_{fuel} and MSR [45] are as follows:

$$E_{fuel} = M_m \times LHV_m + M_d \times LHV_d \quad (4)$$

$$MSR = \frac{100 \times M_m \times LHV_m}{M_m \times LHV_m + M_d \times LHV_d} [\%] \quad (5)$$

In the formula, M_m and M_d represent the mass of methanol and diesel directly injected into the cylinder; LHV_m and LHV_d are defined as the lower heating value of methanol and diesel separately.

3.1. Effects of Injection Location

Studies have shown that the matching degree of diesel/methanol spray, airflow, and chamber affects the engine performance significantly. Generally, the methanol injection location has an impact on the interaction between diesel and methanol spray, thus affecting its atomization effect and mixture homogeneity. In this study, the injection location is characterized by nozzle location, which is defined as the radial nozzle distance r and the axial nozzle distance h , separately, as illustrated in Figure 6. Considering the low energy density of methanol, a high injection rate should be guaranteed by increasing the nozzle diameter and injection pressure. However, due to the poor lubricity and corrosion of methanol to the injection system, it is unwise to increase methanol injection pressure. Thus, a certain methanol injection pressure is compromised, and the nozzle diameter is increased to meet the requirements of methanol injection rate. Simultaneously, in order to ensure that the methanol can overcome environmental backpressure and be directly injected into the cylinder smoothly, the injection pressure should not be too small. Correspondingly, the methanol injection duration and methanol injection pressure are kept constant at 10 °CA and 16 MPa separately. The diesel injection location is set to be 1 mm from the central axis of the injector and 5 mm from the subsurface of the cylinder head. To adjust the injection location, the distance between the methanol nozzles, the central axis of the injector, and the subsurface of the cylinder head is changed. The calculation schemes of the methanol injection location are listed in Table 5.

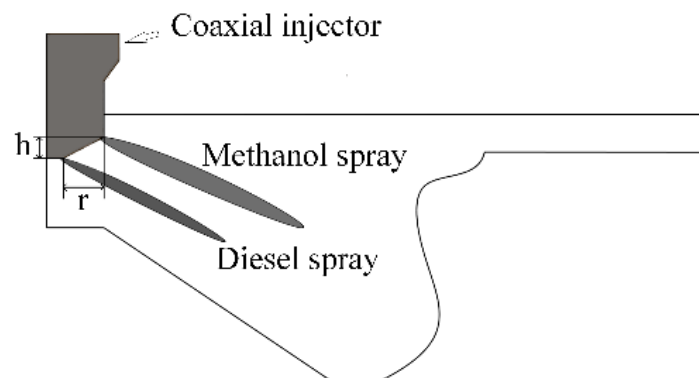


Figure 6. Definition of injection location.

Table 5. Calculation schemes of the methanol injection location.

Nozzle Parameters	Case 1	Case 2	Case 3	Case 4	Case 5	Case 6
Radial nozzle distance r (mm)	0.5	1	1.5	2	2.5	3
Axial nozzle distance h (mm)	0.5	1	1.5	2	2.5	3

3.1.1. Effects of Radial Nozzle Distance r

The axial nozzle distance h is fixed at 4 mm. The distance between the methanol nozzles and the subsurface of the cylinder head is fixed at 1 mm. To investigate the effect of radial nozzle distance r on the engine, the distance between the methanol injection location and the central axis of the injector is adjusted. Three injection intervals (2 °CA, 4 °CA, and 6 °CA) are set as a horizontal comparison. However, it is found that under a 2 °CA injection interval, the engine is prone to rough combustion, while under a 6 °CA injection interval, the engine economy is generally lower than the 4 °CA injection interval after trial calculation. For the coaxial diesel/methanol injector, the reduced injection interval results in more methanol being directly injected toward the diesel jet flame, and methanol is quickly ignited by the diesel, resulting in an improvement in the engine economy. Therefore, the 4 °CA injection interval is selected as the main research case, i.e., D_{SOI} and M_{SOI} are −12 °CA ATDC and −8 °CA ATDC, respectively. The injection intervals of 2 °CA and 6 °CA are used as reference cases.

As observed from Figure 7, the radial nozzle distance r has little effect on the self-ignition of micro-pilot diesel, mainly affecting the diffusion combustion of methanol, which is reflected in the variation of P_{max} and HRR peak. With a larger radial nozzle distance r , the P_{max} is increased and the phase is advanced. The 2 mm radial nozzle distance r corresponds to the highest HRR peak, and the combustion phase is the earliest, followed by 2.5 mm; the lowest peak HRR is caused under the 3 mm radial nozzle distance r . This is because when the radial nozzle distance r is small, although the injection angles of the two fuels are the same, part of the methanol directly injected into the diesel spray is ignited by the micro-pilot diesel quickly, thus enhancing the combustion in the cylinder. Besides, a large amount of heat is taken away in the compression combustion process due to partial methanol spray evaporating with basically the same injection angle as that of diesel spray, when r is smaller than 2 mm, thereby weakening the combustion. However, with the increase in the radial nozzle distance r , more methanol is injected toward the piston wall, thus reducing the amount of methanol directly injected into the diesel spray, resulting in a decrease in the amount of methanol directly ignited by diesel, reducing the HRR and concentration of fuel. Therefore, only a moderate radial nozzle distance is conducive to combustion.

As depicted in Figure 8a, only a slight difference can be observed in the peak of the pressure rise rate, which is similar to the effect of radial nozzle distance r on HRR. The 2 mm radial nozzle distance r leads to the highest pressure rise rate, followed by 2.5 mm and 3 mm. From Figure 8b, it can be summarized that the variation trend in the mean temperature is consistent with the in-cylinder pressure under different radial nozzle distances. The radial nozzle distance r has little effect on the mean temperature before TDC. However, the mean temperature increases slightly with the increase in the radial nozzle distance r after TDC, which increases the exhaust losses. The increased thermal losses deteriorate the thermal efficiency, leading to more carbon emission [46]. When a 3 mm radial nozzle distance r is adopted, the mean temperature reaches the maximum among the six cases. Since the compression of the piston and the self-ignition of diesel lead to the variation of in-cylinder pressure before TDC, which depends on the compression ratio of the engine and the ignition characteristics of diesel, the influence of the radial nozzle distance r can almost be neglected. When the compression stroke comes to an end, the existence of the surrounding low-pressure zone leads to rapid evaporation of the methanol spray and the formation of a homogeneous mixture after TDC. At the same time, more methanol

impinges on the piston wall with a longer radial nozzle distance r , which accelerates the breakup of the spray, promoting the formation of a homogeneous mixture.

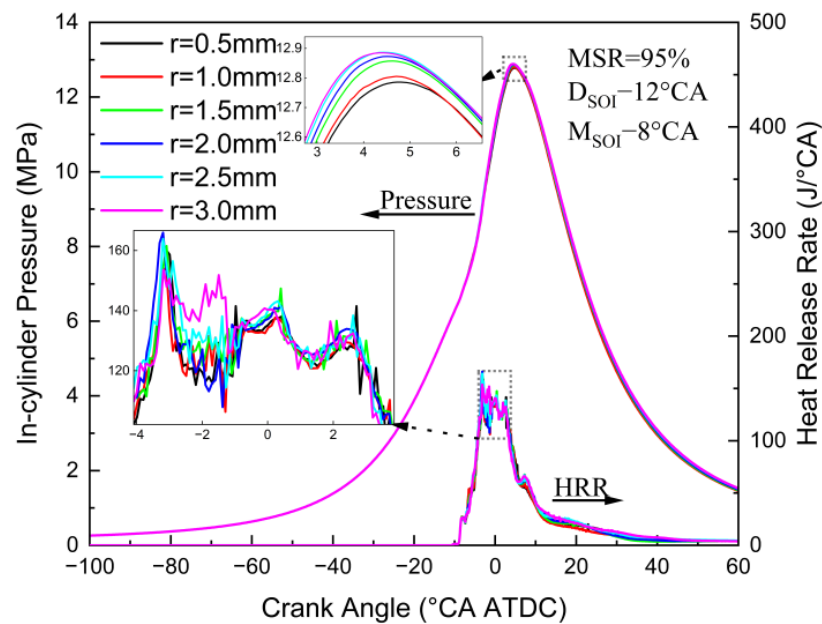


Figure 7. Pressure and HRR curves for various radial nozzle distances.

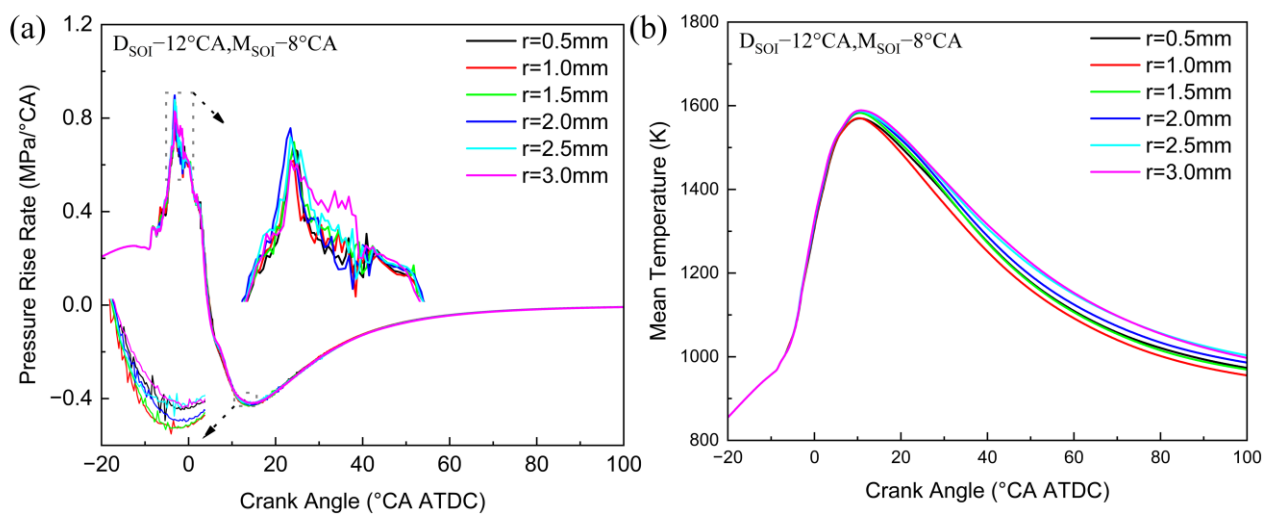


Figure 8. Effects of different radial nozzle distances on (a) pressure rise rate, (b) and mean temperature.

CA50 refers to the crank angle (CA) when the fuel heat release reaches 50% of the E_{fuel} . Ignition delay refers to the period between D_{SOI} and the CA, when 10% E_{fuel} is released. The combustion duration (CA10–CA90) represents the duration of the E_{fuel} released from 10% to 90%.

As shown in Figure 9, the radial nozzle distance r has little influence on CA50, ignition delay, and CA10–CA90, along with no obvious variation trend among the six cases. The CA50 and CA10–CA90 reduce slightly, and the ignition delay increases slightly at the 2 °CA injection interval, with the increase in radial nozzle distance r . When adopting the 4 °CA injection interval, with the increase in the radial nozzle distance r , the CA50 first decreases, then increases, and finally decreases; the CA10–CA90 decreases gradually, and the ignition delay remains basically unchanged. The CA50 increases, the ignition delay stays constant,

and the CA10–CA90 first increases and then decreases with the radial nozzle distance r increasing when the 6 °CA injection interval is adopted. Consequently, the influence of the injection interval on combustion characteristics is much larger than r . With the increase in the injection interval, CA50 is delayed, the ignition delay is increased, and the CA10–CA90 is prolonged. On the one hand, the evaporation of methanol is affected by the injection interval directly before TDC, determining the homogeneity of the combustible mixture, which impacts the in-cylinder combustion significantly before diesel ignition. On the other hand, the interaction between methanol spray and diffused diesel flame is weakened when a larger injection interval is adopted, thus delaying the overall combustion heat release.

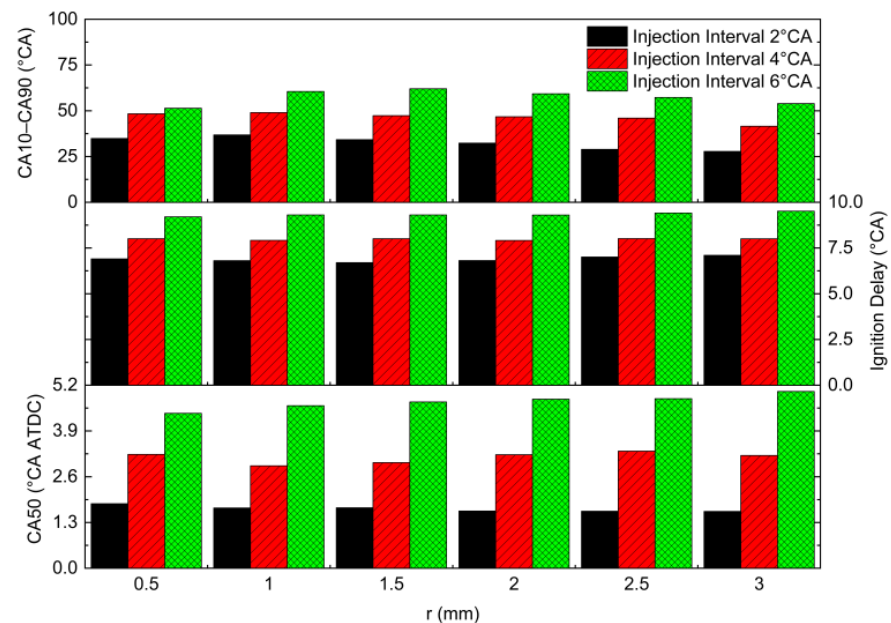


Figure 9. Effects of different radial nozzle distances on CA50, ignition delay, and CA10–CA90.

The mixture homogeneity is analyzed based on the distribution of the in-cylinder fuel/air equivalent ratio. The penetration distance is defined as the length of fuel injected from the nozzles to the cylinder.

As observed from Figure 10, the distribution of the equivalent ratio in the cylinder is affected significantly by the radial nozzle distance r under different crank angles. The penetration distance increases and the enriched area in front of the spray decreases with the increase in radial nozzle distance r . This is because the larger radial nozzle distance r weakens the interaction of methanol and diesel spray, and more methanol is injected directly toward the piston wall, as a result of which the mixing homogeneity of the front end of the spray is improved. Moreover, the enriched area diffuses from the middle of the chamber to the piston pit gradually as the piston goes down. Meanwhile, the enriched area is distributed in the middle of the chamber when the radial nozzle distance r is 0.5 mm and 1 mm; when the radial nozzle distance r is 2.5 mm and 3 mm, the enriched area transfers to the piston pit with a heterogeneous mixture; when the radial nozzle distance r is 2 mm, there is no too enriched or too lean area in the chamber, making 2 mm the case with the highest mixture homogeneity, which is consistent with the influence of the radial nozzle distance r on HRR. Therefore, a moderate radial nozzle distance should be adopted to improve fuel mixing.

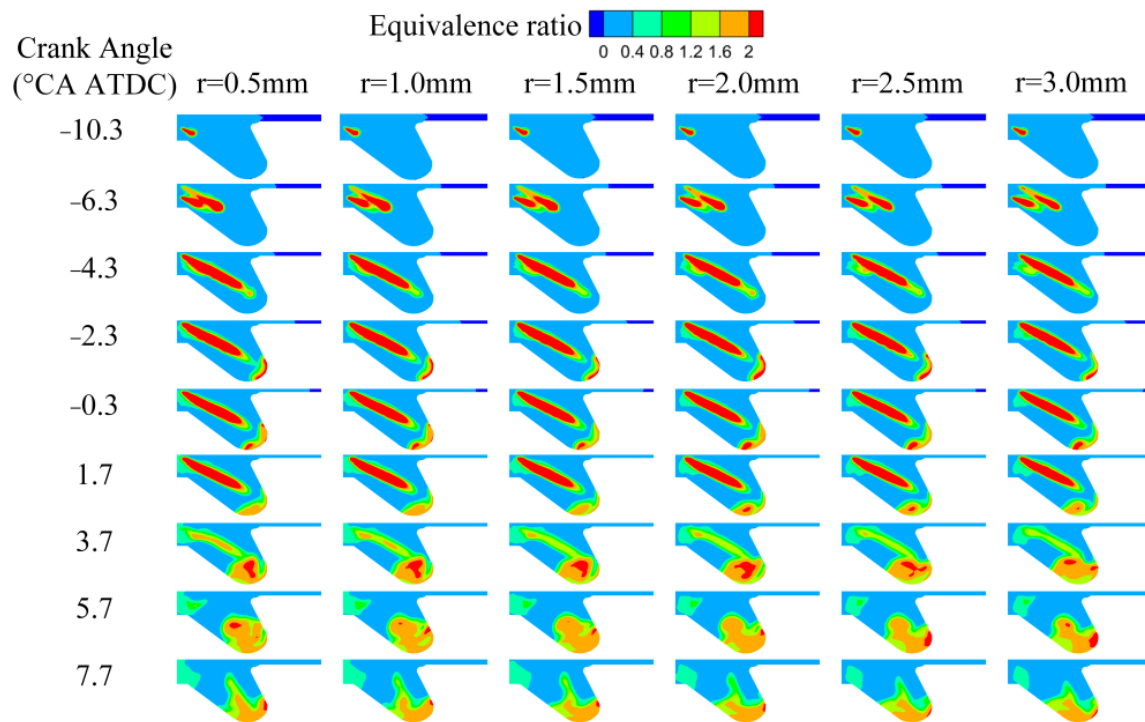


Figure 10. Equivalent ratio of different radial nozzle distances.

Figure 11 displays the comparisons of NO_x , soot, HC, and CO emissions at six radial nozzle distances. It can be seen that the exhaust emissions vary greatly with different injection intervals. With the increase in the injection interval, the emissions of soot and CO increase, while the emission of NO_x decreases. This is because the increased injection interval reduces the mixing time of diesel spray and methanol spray, which increases the concentration of the mixture, contributing to more soot emission and less NO_x emission. When adopting the radial distance of 1 mm, there exists a turning point in the NO_x , soot, HC, and CO emissions under 4 °CA injection interval. The NO_x emission reduces first and then increases with the increase in the radial nozzle distance r , whereas the emissions of soot, HC, and CO first increase and then decrease. This can be explained as follows. The 1 mm radial nozzle distance r corresponds to a larger enriched area in the cylinder, wherein incomplete combustion is prone to be caused by an environment with lean air, increasing the soot, HC, and CO emissions. However, the NO_x emission is inhibited in the anoxic environment, causing a reduction in NO_x emissions. Therefore, a moderate radial nozzle distance r should be employed to reduce the NO_x , soot, HC, and CO emissions, which should be weighed to select the radial nozzle distance r . In addition, it is found that the exhaust emissions are relatively low when the 2.5 mm radial nozzle distance is adopted, among which the NO_x emission can meet the IMO Tier II regulations without any after-treatment devices.

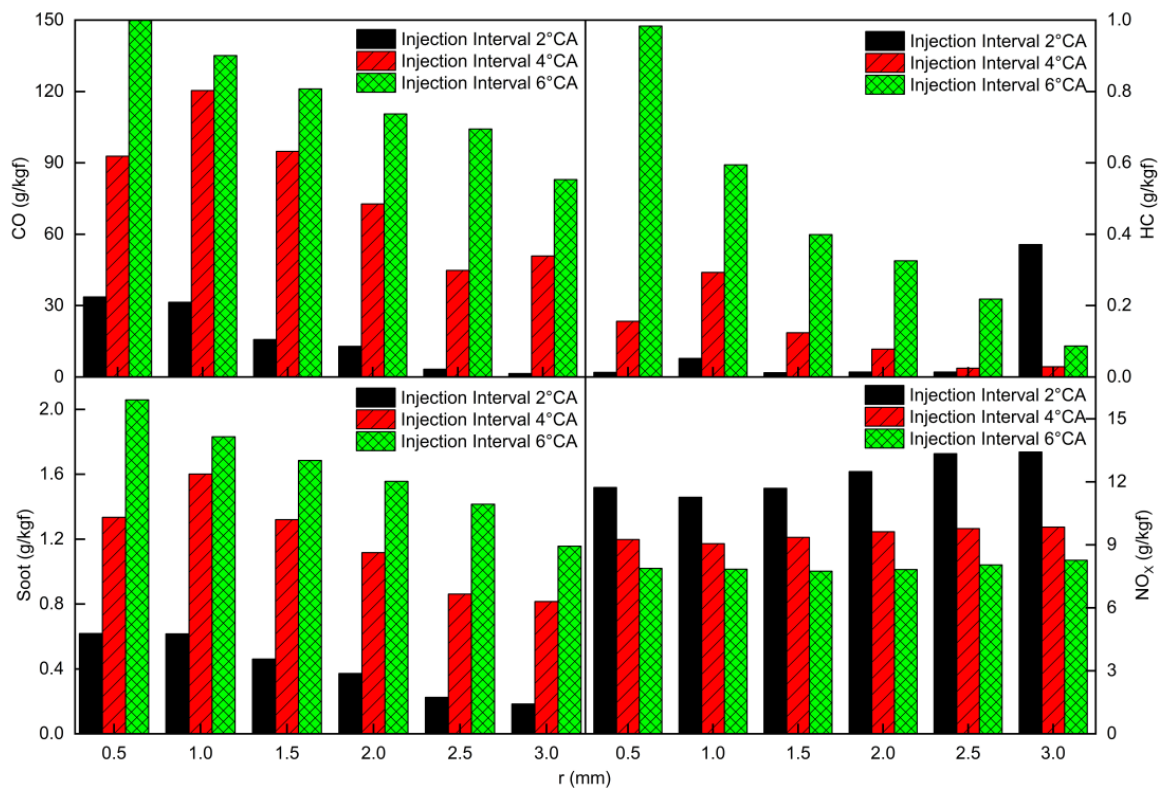


Figure 11. Comparisons of exhaust emissions at various radial nozzle distances.

3.1.2. Effects of Axial Nozzle Distance h

The radial nozzle distance r is fixed at 2.5 mm. The distance from the diesel nozzles to the central axis of the injector is kept at 2.5 mm. The distance between methanol nozzles and the subsurface of the cylinder head is adjusted to explore the influence of axial nozzle distance h on the engine.

It is revealed that the axial nozzle distance h has a slight impact on P_{\max} and peak HRR in Figure 12. Figure 13 presents the pressure rise rate and mean temperature profiles under various axial nozzle distances h . In Figure 13a, the trend of pressure rise rate under six different axial nozzle distances h is consistent. Only the peak differs slightly for the diffusion combustion of the methanol, and 2.5 mm corresponds to the highest peak among the six cases. However, 3 mm corresponds to a longer duration of obtaining a higher pressure rise rate, leading to the highest P_{\max} . In Figure 13b, the mean temperature of the six cases is almost identical in the compression stage and the initial stage of combustion. The mean temperature corresponding to different axial nozzle distances h increases as the piston moves down; 3 mm leads to the highest mean temperature, followed by 2.5 mm, indicating that a higher in-cylinder temperature is obtained in the expansion stroke with the increase in the axial nozzle distance h , which contributes to improvements in the combustion characteristics. This is because 3 mm corresponds to the largest ignition delay, the most delayed CA50, and the longest CA10–CA90, which postpones the phase of the combustion, thus increasing the temperature in the expansion stroke (Figure 14).

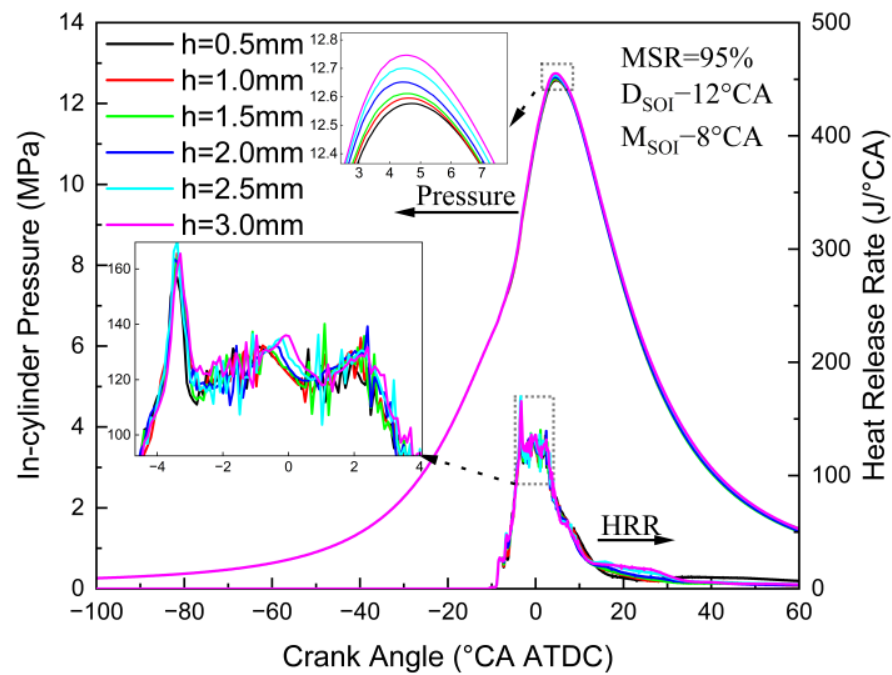


Figure 12. Pressure and HRR curves for various axial nozzle distances h .

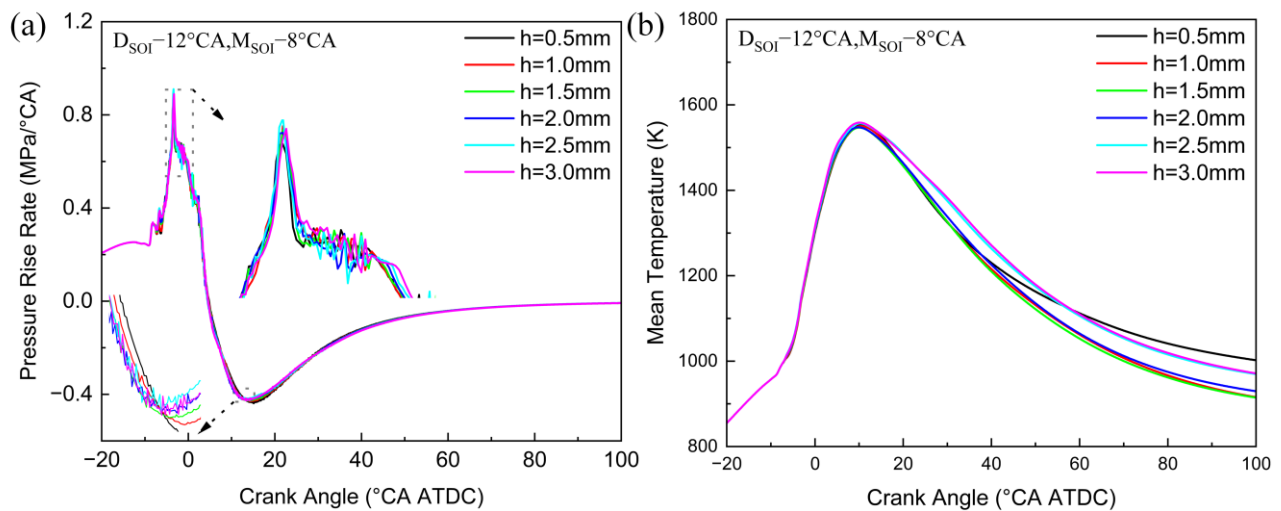


Figure 13. Effects of different axial nozzle distances h on (a) pressure rise rate, (b) and mean temperature.

Figure 14 shows the influence of six axial nozzle distances h on CA50, ignition delay, and CA10–CA90 under three different injection intervals. As can be seen from Figure 14, the combustion characteristics are slightly affected by h , but are significantly influenced by the injection interval, especially the CA50, which has an effect similar to that of r . With the increase in the injection interval, CA50 is delayed, the ignition delay is increased, and the CA10–CA90 is prolonged. This is because the increased injection interval causes less methanol spray to burn with the diesel spray ignited by compression, thus decreasing the combustion rate.

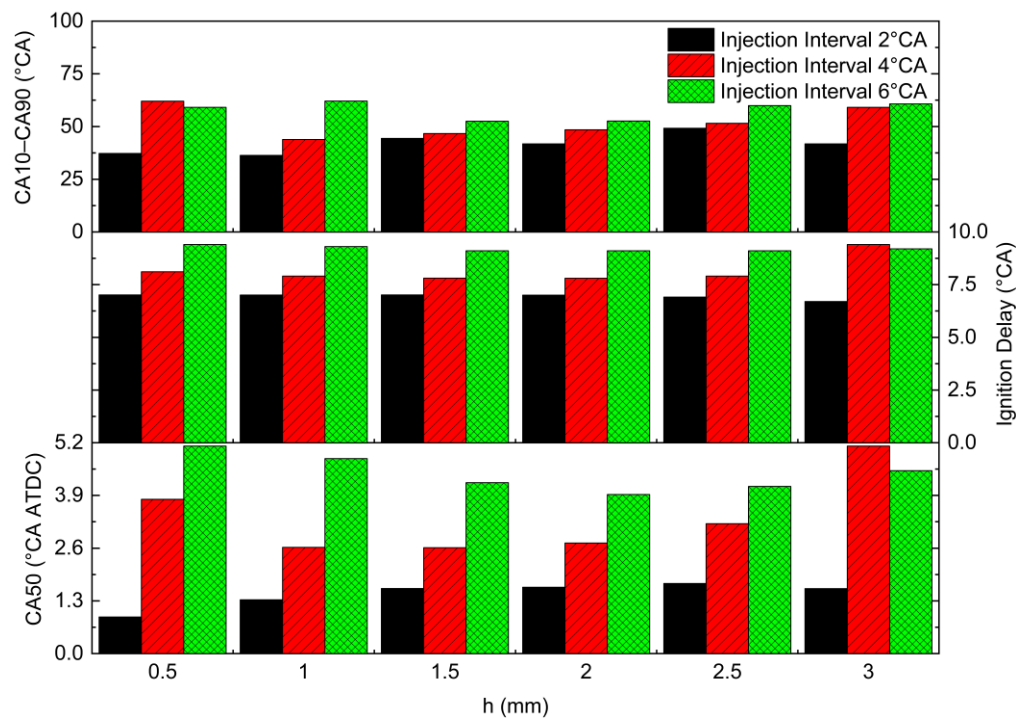


Figure 14. Effects of different axial nozzle distances h on CA50, ignition delay, and CA10–CA90.

Figure 15 illustrates the in-cylinder distribution of the fuel/air equivalent ratio under six different axial nozzle distances h . As illustrated in Figure 15, with the increase in the axial nozzle distance h , the enriched area in the front of the spray and its surroundings decreases, improving the mixture homogeneity. Besides, the enriched area is transferred from the piston wall to the piston pit gradually, making the homogeneous area mainly distributed in the central section of the piston pit. One of the reasons is that the increase in the axial nozzle distance h reduces the interaction of methanol and diesel spray, promoting the mixing of methanol and air. The second reason is that the smaller axial nozzle distance h increases the penetration distance of the spray, as a result of which the enriched fuel in front of the spray first reaches the piston pit at -3.8°CA ATDC , and a mass of fuel is splashed onto the piston wall and cooled to a certain extent, deteriorating the mixture homogeneity in the piston pit.

Figure 16 presents the effects of six different axial nozzle distances h on the emissions of NO_x , soot, HC, and CO. As depicted in Figure 16, the emissions of NO_x , soot, HC, and CO differ significantly under various axial nozzle distances h . The impact of injection interval on emissions at different h is similar to r . For the 4°CA injection interval, the NO_x emission decreases initially, followed by an increase with the increase in the axial nozzle distance h , while the emissions of soot, HC, and CO act oppositely, revealing that there is a turning point in the trend of the emissions. Two reasons may account for the turning point. On the one hand, $h = 1\text{ mm}$ leads to a relatively low oxygen concentration, which inhibits NO_x emission (Figure 15). On the other hand, the incomplete combustion appearing in the unburned methanol regions is more obvious when the axial nozzle distance h increases; this is the source of the increased HC and CO emissions. Additionally, it is found by weighing the NO_x , soot, HC, and CO emissions that the best emission effects can be achieved with a 0.5 mm axial nozzle distance h .

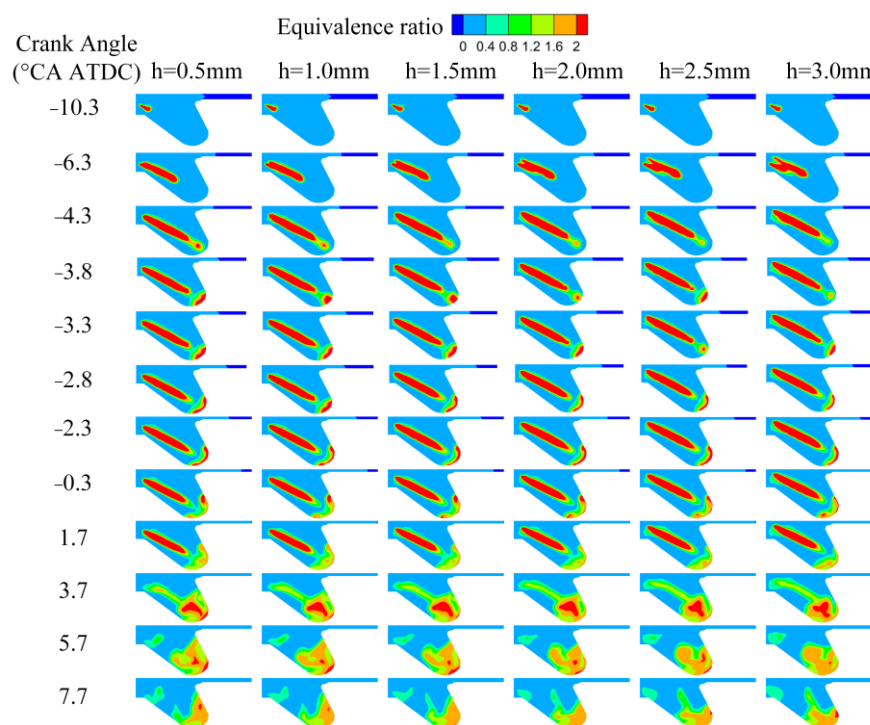


Figure 15. Equivalent ratio of different axial nozzle distances h .

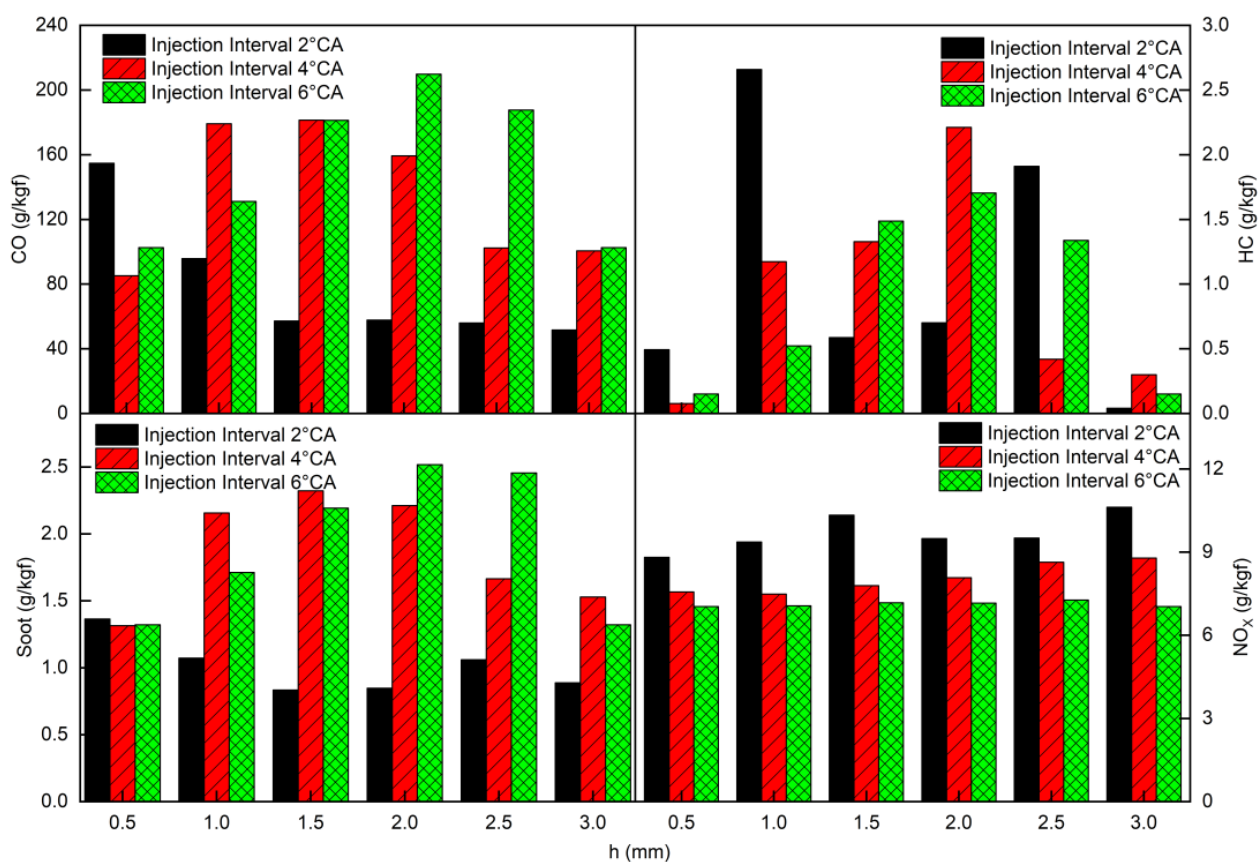


Figure 16. Comparisons of exhaust emissions at different axial nozzle distances h .

Overall, the effect of the methanol injection location on combustion is relatively insignificant. Nevertheless, a moderate methanol injection location contributes to the improvement of the mixture homogeneity, leading to lower overall exhaust emissions. To achieve the lowest overall exhaust emissions, the optimal radial nozzle distance r and the axial nozzle distance h of 2.5 mm and 0.5 mm, respectively, are selected for the following study.

3.2. Effects of Methanol Injection Duration and Methanol Injection Pressure

The methanol injection pressure depends on methanol injection mass, injection duration, nozzle numbers, and nozzle diameters. Once the methanol injection mass is determined, the other four parameters affect each other. The mass of methanol injected per cycle is kept constant by fixing E_{fuel} and MSR. According to the specifications of the engine and the requirement of injection rate, the nozzle numbers and nozzle diameters are determined. Therefore, there is a matching relationship between the methanol injection duration and injection pressure, based on which six typical combined cases of methanol injection duration and methanol injection pressure are designed to explore their effects on the engine combustion characteristics, mixture homogeneity, and exhaust emissions. The six combined cases are shown in Table 6.

Table 6. Combined cases of methanol injection strategies.

Simulation Cases	Injection Duration (°CA)	Injection Pressure (MPa)
Case 7	5	64
Case 8	6	44.4
Case 9	7	32.7
Case 10	8	25
Case 11	9	19.8
Case 12	10	16

Figure 17 plots the in-cylinder pressure and HRR comparisons of six combined cases of methanol injection duration and methanol injection pressure. Generally, with the increase in methanol injection duration and the decrease in methanol injection pressure, the in-cylinder pressure and HRR decrease accordingly, under 95% high MSR. On the one hand, the longer injection duration strengthens the inhibition action of the high vaporization latent heat of methanol on the increase in in-cylinder temperature, thus reducing the in-cylinder explosion pressure. On the other hand, the lower injection pressure suppresses the breakup and atomization of methanol spray, thus slowing down the combustion rate and leading to a lower P_{max} and peak HRR. In addition, methanol converts high-activity OH to low-activity H_2O_2 below 1000 K, reducing the reactivity at the initial stage of combustion [47]. Among the six cases, two HRR peaks caused by diesel self-ignition and methanol diffusion combustion, respectively, are observed. Compared with the first peak, the second peak is more sensitive to methanol injection duration, which arises from the variation in the concentration and the rate of methanol diffusion combustion.

Figure 18 gives the pressure rise rate and in-cylinder mean temperature curves corresponding to the six combined cases of methanol injection duration and methanol injection pressure, respectively. As illustrated in Figure 18, the pressure rise rate and in-cylinder mean temperature show an increasing trend with the decrease in methanol injection duration and the increase in methanol injection pressure, which is in agreement with the in-cylinder pressure and HRR. Case 7 produces the highest pressure rise rate and mean temperature for two reasons. Firstly, methanol is allowed to be completely injected with a shorter injection duration and larger injection pressure before TDC in the compression stroke, wherein the pressure and temperature rise sharply with a high constant combustion volume, thus improving the engine thermal efficiency and fuel economy. Then, the higher injection pressure improves the atomization of methanol, which promotes the diffusion combustion of methanol near TDC. Therefore, a shorter injection duration matching a

higher injection pressure is conducive to improving the engine economy. However, considering that the peak pressure rise rate reached $1.39 \text{ MPa}/^\circ\text{CA}$ under a methanol injection pressure of 64 MPa (case 7), the combustion tends to be rough as the methanol injection pressure continues to increase. In addition, the sharply increased in-cylinder mean temperature with the increase in the methanol injection pressure can increase the emission of NO_x significantly. Therefore, methanol injection strategies for high-efficiency and low-emission combustion need to be weighed.

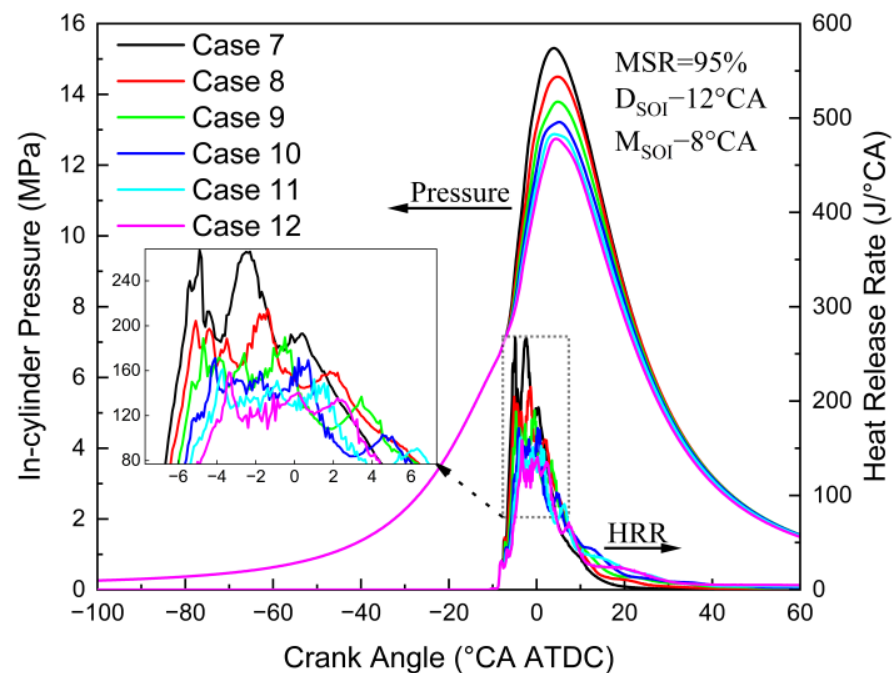


Figure 17. Pressure and HRR curves for various methanol injection durations and methanol injection pressures.

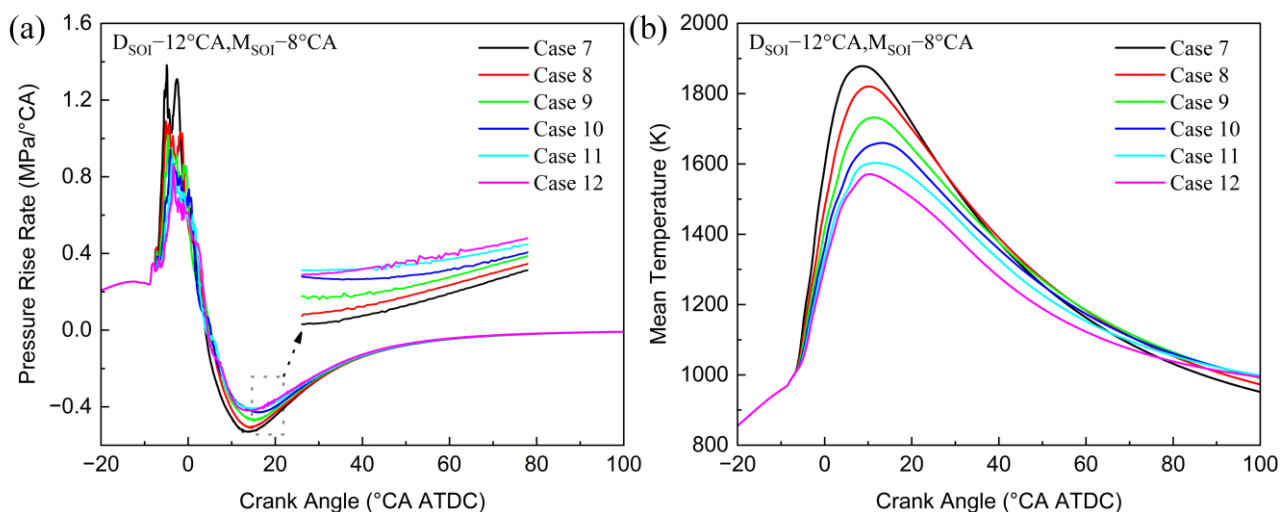


Figure 18. Effects of various methanol injection durations and methanol injection pressures on (a) pressure rise rate, (b) and mean temperature.

Figure 19 illustrates the effects of methanol injection duration and methanol injection pressure on CA50, ignition delay, and CA10–CA90 under six different cases. As summarized in Figure 5, the ignition delay and CA10–CA90 increase with the methanol

injection duration prolonged and injection pressure reduced under three different injection intervals. The ignition delay increases with the injection interval increasing, which is relatively inconspicuous compared with the influence of the injection interval on CA50 and CA10–CA90. On the one hand, the reduction in injection pressure deteriorates the atomization of methanol spray, thus delaying the combustion phase. Meanwhile, partial methanol is injected into the cylinder in the expansion stroke with the injection duration prolonged, which reduces the concentration of combustion and heat release, thus leading to an increase in CA10–CA90. On the other hand, since both diesel and methanol are injected near TDC with high in-cylinder temperature, the heat absorbed by methanol vaporization latent heat is weakened, so the ignition delay in each case is almost identical. Furthermore, a turning point exists in CA50 corresponding to injection intervals of 2 °CA and 4 °CA. There is a trend of first decreasing and then increasing with the increase in methanol injection duration and the decrease in injection pressure, which is more apparent in the 2 °CA injection interval. This is because when the injection interval is small, micro-pilot diesel is injected first, and methanol is subsequently injected. At the same time, diesel begins to be compressed with low in-cylinder temperature, while methanol with a high latent heat of vaporization is injected into the cylinder, absorbing a mass of heat, delaying the combustion, and causing CA50 to move backward. The heat of the diesel generated by the compression ignition is enough to ignite the methanol with the injection interval increasing, as a result of which the effect of methanol vaporization and heat absorption can be ignored. When the 6 °CA injection interval is adopted, the turning point disappears. With the increase in methanol injection duration, the injection pressure decreases, and CA50 keeps increasing, indicating that the main heat release phase deviates from TDC gradually, the constant combustion volume decreases, the engine thermal efficiency decreases, and the fuel economy deteriorates.

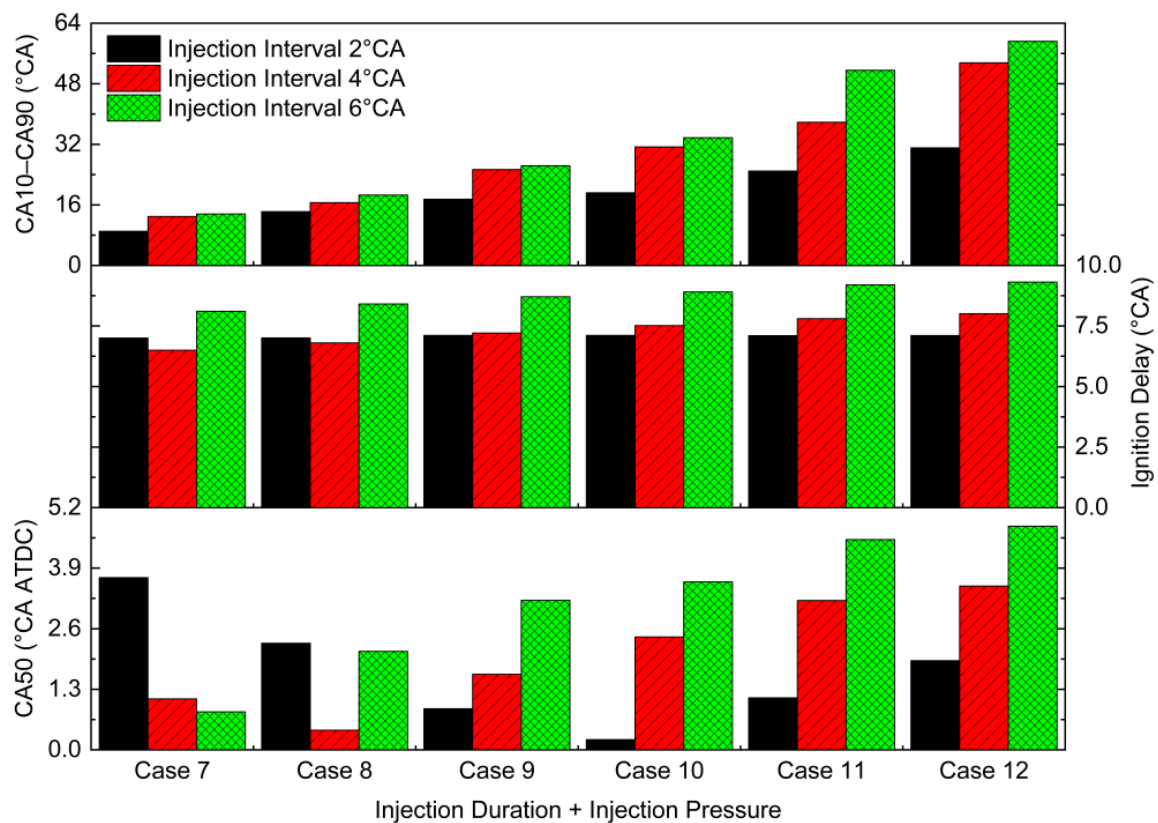


Figure 19. Comparisons of CA50, ignition delay, and CA10–CA90 under different methanol injection durations and methanol injection pressures.

As depicted in Figure 20, case 7 leads to the best mixture homogeneity among the six cases. In case 7, the spray impinges on the chamber wall and rebounds, forming a mass of homogeneous mixture in the central section of the piston pit. In general, longer spray penetration distance avoids the appearance of lean and enriched areas near CA50. This is because the higher injection pressure accelerates the breakup and atomization of methanol, improving the mixing effect of fuel and air. Moreover, it can be seen from the spatial distribution of the equivalent ratio that the enriched area first appears in the center of the spray, while the outer layer of the spray which evaporates first and then contacts the in-cylinder air is more homogeneous. Then, the enriched spray is injected toward the piston pit, where the spray further breaks up and continuously diffuses to the central section of the chamber, leading to a homogeneous mixture.

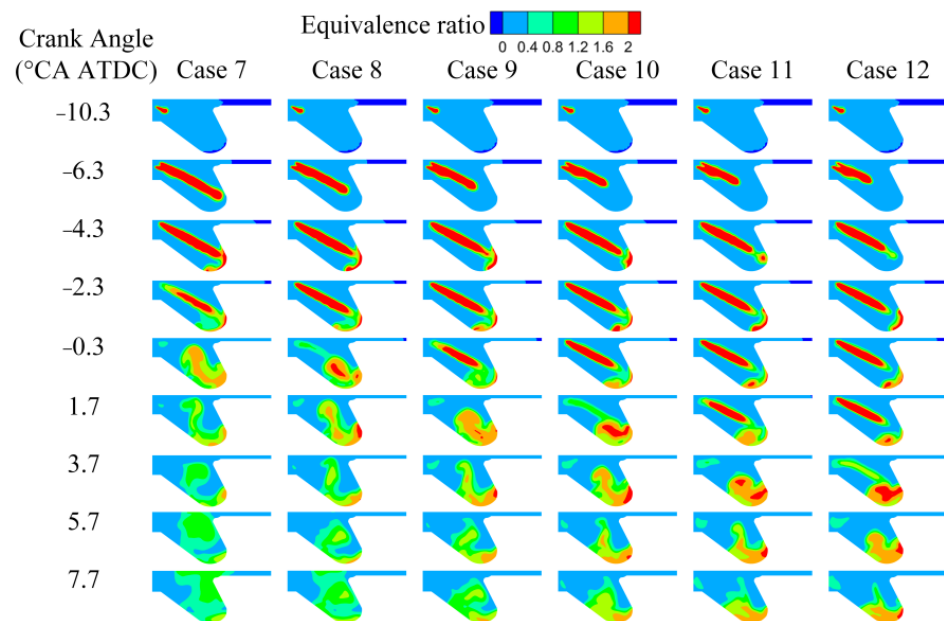


Figure 20. Equivalent ratio of different methanol injection durations and methanol injection pressures.

The NO_x emission is reduced with the increase in methanol injection duration and the reduction in methanol injection pressure under three injection intervals, while the trend of soot emission is exactly the opposite, as summarized in Figure 21. The difference in the formation mechanism of NO_x and soot makes it difficult to break up the trade-off relationship, whereas the current cases have achieved lower NO_x and soot emissions, and the optimal case can meet the IMO Tier II limit requirement. Additionally, HC and CO emissions also follow a similar trend. With the prolongation of methanol injection duration and the reduction in methanol injection pressure, trends of decreasing and increasing are observed, respectively. It is noteworthy that when the injection interval is 4 °CA and 6 °CA, a shorter injection duration matching a larger injection pressure leads to an ultra-low HC emission with almost zero exhaust emission. This is because as the injection interval increases, the injection of methanol is delayed, and closer to the top dead center. At this time, the higher in-cylinder temperature provides good conditions for methanol evaporation. Due to its high vaporization latent heat value, the heat absorption of methanol evaporation reduces the temperature inside the chamber, resulting in a decrease in HC emissions. Simultaneously, with the increase in the injection interval, the NO_x emissions decrease, while the soot emissions increase, which is caused by the decreased in-cylinder temperature and the deteriorating mixture homogeneity between methanol spray and air. When the injection interval is 2 °CA, the CO emission is relatively low, which fully demonstrates the advantages of in-cylinder direct injection methanol in reducing exhaust emissions, especially in carbon emission reduction.

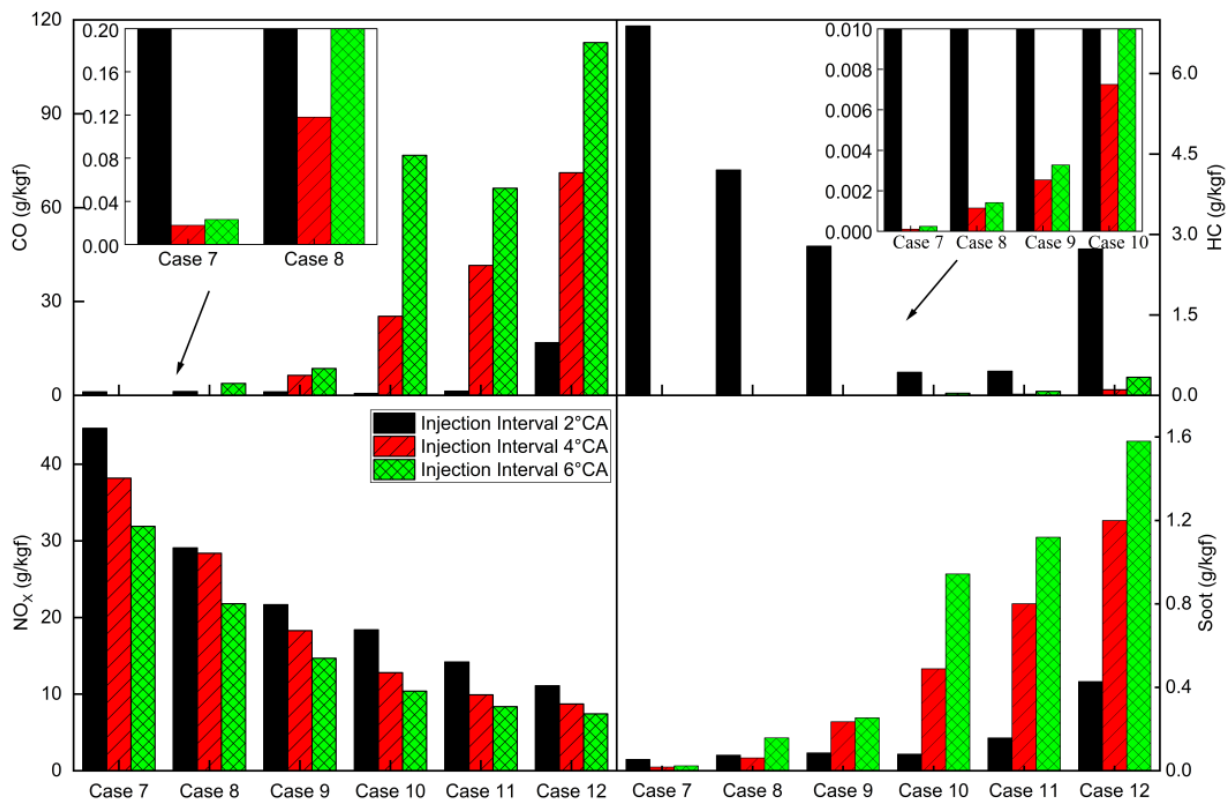


Figure 21. Comparisons of exhaust emissions under different methanol injection durations and methanol injection pressures.

3.3. Analysis and Determination of the Optimal Injection Strategy

In this section, the combustion efficiency (CE), equivalent indicated specific fuel consumption (EISFC), and indicated thermal efficiency (ITE) are analyzed to evaluate different injection strategies and determine the optimal injection strategy based on the above conclusions. Considering that the radial nozzle distance r and axial nozzle distance h have little effect on combustion characteristics, only the influence of methanol injection duration and injection pressure on CE, ITE, and EISFC are analyzed in this section. CE is an important indicator to evaluate whether the fuel is fully combusted [21]. EISFC and ITE are used to evaluate the engine economy. The definition of CE, EISFC, and ITE are as follows:

$$CE = 100 * \left(1 - \frac{M_{CO} \times LHV_{CO} + M_{HC} \times LHV_d + M_m \times LHV_m}{M_d \times LHV_d + M_m \times LHV_m} \times W_i \right) [\%] \quad (6)$$

$$EISFC = \frac{M_d \times LHV_d + M_m \times LHV_m}{W_i \times LHV_d} \quad (7)$$

$$ITE = \frac{100 \times W_i}{M_d \times LHV_d + M_m \times LHV_m} [\%] \quad (8)$$

where W_i is the indicated work. M_{CO} and M_{HC} represent the mass of CO and HC emissions, respectively. LHV_{CO} represents the lower heating value of CO.

Figure 22 shows the effects of six different methanol injection strategies on CE, EISFC, and ITE. It can be seen from Figure 22a that the injection interval has significant effect on CE, ITE, and EISFC. With the increase in the injection interval, CE and EISFC are increased, while ITE is decreased, deteriorating the engine economy. Case 8 corresponds to the lowest CE, and case 12 the highest CE, in the injection interval of 4 °CA; however, the difference between the two cases is only 0.009%. Thus, it can be seen that the impact of the methanol injection strategy on CE is relatively small among the six cases. However, EISFC and ITE are

significantly influenced by the injection strategy, showing an opposite trend under different cases (Figure 22b). Case 8 corresponds to the lowest EISFC and the highest ITE, which differ by 11.2% and 12.6% from case 12. Additionally, the values for ITE and EISFC are almost the same in case 8 under different injection intervals. Therefore, the optimal emission and economy are obtained with the methanol injection duration of 6 °CA, matching an injection pressure of 44.4 MPa (case 8). However, considering the poor lubricity and the corrosive nature of methanol, it is worth noting that this high injection pressure could lead to unwanted consequences under real-life conditions, e.g., corrosion, increased wear, and fuel leakage issues.

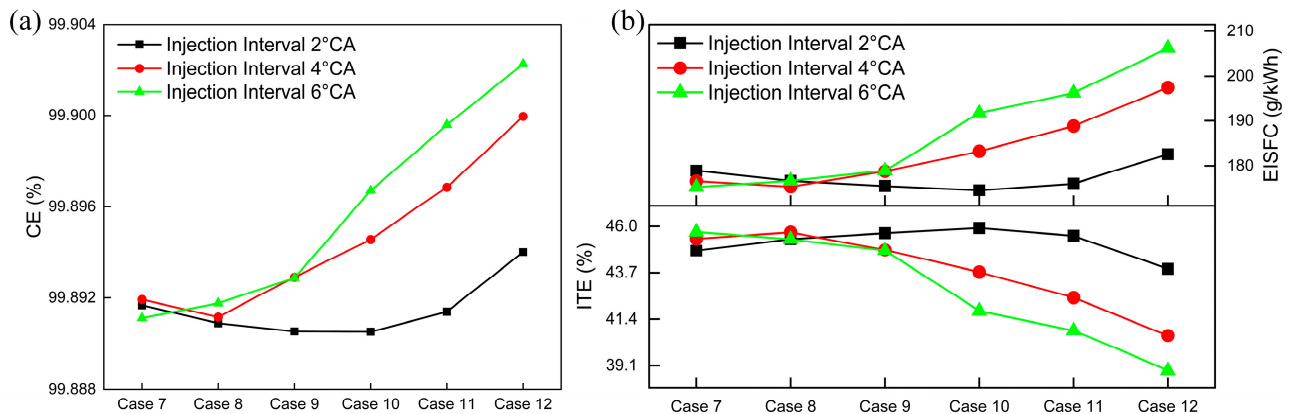


Figure 22. Effects of different methanol injection strategies on engine performance. (a) Combustion efficiency; (b) equivalent indicated specific fuel consumption and indicated thermal efficiency.

4. Conclusions

In the study, a 3-D CFD model of a high-pressure direct injection diesel/methanol dual-fuel engine is established. Additionally, the influences of methanol injection location, injection duration, and injection pressure on engine combustion characteristics, mixture homogeneity, and emissions are investigated at the rated speed of 1660 r/min and the engine load of 75%, based on the numerical model, which provides theoretical guidance for the development and design of high-pressure direct injection diesel/methanol dual-fuel engines, from the time and space perspective. Based on the simulation results, the main findings are summarized as follows:

1. The radial nozzle distance r is conducive to improving the engine performance after weighing. The P_{max} increases slightly, the peak HRR increases first and then decreases, and the in-cylinder mean temperature in the expansion stroke increases significantly with the increase in the radial nozzle distance r . A turning point (with minimum NO_x emission) is achieved when r is 1 mm at the 4 °CA injection interval, while the emissions of soot, HC, and CO correspondingly reach a peak. Overall, the lowest emissions of NO_x , soot, CO, and HC are achieved with a 2.5 mm radial nozzle distance r , where the NO_x emissions meet the IMO Tier II regulations without any after-treatment measures.
2. The axial nozzle distance h has a subtle impact on the in-cylinder pressure and HRR, with a slight difference at the peak, which is similar to the radial nozzle distance r . With the increase in the axial nozzle distance h , the enriched areas around the spray decrease, and the homogeneous mixture in the central section of the piston pit increases, which improves the mixture homogeneity. However, the injection interval has a greater impact on combustion characteristics than r and h . A larger injection interval leads to a delayed CA50, increased ignition delay, and prolonged CA10–CA90. Additionally, the fuel is burned completely when h is 0.5 mm, leading to optimal emission characteristics.

3. The methanol injection duration and methanol injection pressure have dramatic impacts on combustion characteristics, mixture homogeneity, and emissions. A shorter methanol injection duration matching a higher injection pressure can lead to a higher P_{\max} and peak HRR along with a shorter ignition delay and CA10–CA90, thus improving the thermal efficiency and fuel economy significantly. With the increase in injection duration and the reduction in injection pressure, the CA50 first approaches and then moves away from the TDC, but the trend of approaching the TDC is weakened with the increase in the injection interval.
4. The shorter injection duration and higher injection pressure accelerate the breakup and atomization of methanol spray, which improves the mixture homogeneity, causing lower emissions of soot and CO, but higher emissions of NO_x. Besides, with the increase in the injection interval, the emission of HC is decreased, while CO is increased under different injection durations and injection pressures.
5. The increased injection interval under different methanol injection durations and injection pressures leads to higher CE and EISFC, but lower ITE, deteriorating the engine economy. The optimal emission characteristics and economy are obtained when matching an injection duration of 6 °CA, with an injection pressure of 44.4 MPa. The ITE is increased in this case compared to the other injection strategies, thereby improving the engine performance significantly. However, unwanted potential issues such as corrosion, increased wear, and fuel leakage may be caused in real-life conditions with this high injection pressure, due to the poor lubricity and the corrosive nature of methanol.

Author Contributions: Conceptualization, H.W., Y.Y., J.L. and C.X.; methodology, H.W. and Y.Y.; software, J.L., Y.Y. and C.X.; validation, J.L. and Y.Y.; formal analysis, Y.Y.; investigation, H.W., Y.Y., J.L., C.X., H.J. and J.S.; resources, H.W. and Y.Y.; data curation, Y.Y.; writing—original draft preparation, Y.Y.; writing—review and editing, H.W., J.L. and C.X.; visualization, Y.Y.; supervision, H.W., Y.Y., J.L. and C.X. All authors have read and agreed to the published version of the manuscript.

Funding: This research received no external funding.

Institutional Review Board Statement: Not applicable.

Informed Consent Statement: Not applicable.

Data Availability Statement: The data presented in this study are available on request from the corresponding author.

Conflicts of Interest: The authors declare no conflict of interest.

Nomenclature

AMR	Adaptive mesh refinement
ATDC	After top dead center
BDC	The bottom dead center
CA10–CA90	Combustion duration
CA50	Crank angle for releasing 50%
CE	Combustion efficiency
CFD	Computational fluid dynamics
E_{fuel}	Total fuel calorific value
EGR	Exhaust gas recirculation
EISFC	Equivalent indicated specific fuel consumption
EVO	Exhaust valve opening
H ₂ O ₂	Hydrogen peroxide

HRR	Heat release rate
IMEP	Indicated mean effective pressure
ITE	Indicated thermal efficiency
IVC	Intake valve closing
LHV_d	Lower heating value of diesel
LHV_m	Lower heating value of methanol
M_{CO}	The mass of CO emission
M_d	Diesel mass
M_{HC}	The mass of HC emission
M_m	Methanol mass
M_{SOI}	Methanol injection timing
MSR	Methanol substitution rate
OH	Hydroxyl radicals
P_{max}	Maximum in-cylinder pressure
SOI	Start of injection
TDC	The top dead center
W_i	Indicated work

References

1. Soni, D.K.; Gupta, R. Optimization of methanol powered diesel engine: A CFD approach. *Appl. Therm. Eng.* **2016**, *106*, 390–398. [\[CrossRef\]](#)
2. Huang, G.; Li, Z.; Zhao, W.; Zhang, Y.; Li, J.; He, Z.; Qian, Y.; Zhu, L.; Lu, X. Effects of fuel injection strategies on combustion and emissions of intelligent charge compression ignition (ICCI) mode fueled with methanol and biodiesel. *Fuel* **2020**, *274*, 117851. [\[CrossRef\]](#)
3. Bayraktar, H. An experimental study on the performance parameters of an experimental CI engine fueled with diesel–methanol–dodecanol blends. *Fuel* **2008**, *87*, 158–164. [\[CrossRef\]](#)
4. Sayin, C. Engine performance and exhaust gas emissions of methanol and ethanol–diesel blends. *Fuel* **2010**, *89*, 3410–3415. [\[CrossRef\]](#)
5. Chen, H.; Su, X.; Li, J.; Zhong, X. Effects of gasoline and polyoxymethylene dimethyl ethers blending in diesel on the combustion and emission of a common rail diesel engine. *Energy* **2019**, *171*, 981–999. [\[CrossRef\]](#)
6. Zhou, Y.; Hong, W.; Yang, Y.; Li, X.; Xie, F.; Su, Y. Experimental Investigation of Diluents Components on Performance and Emissions of a High Compression Ratio Methanol SI Engine. *Energies* **2019**, *12*, 3366. [\[CrossRef\]](#)
7. Liu, Y.; Jiao, W.; Qi, G. Preparation and properties of methanol–diesel oil emulsified fuel under high-gravity environment. *Renew. Energy* **2011**, *36*, 1463–1468. [\[CrossRef\]](#)
8. Gong, C.; Li, Z.; Chen, Y.; Liu, J.; Liu, F.; Han, Y. Influence of ignition timing on combustion and emissions of a spark-ignition methanol engine with added hydrogen under lean-burn conditions. *Fuel* **2019**, *235*, 227–238. [\[CrossRef\]](#)
9. Gong, C.; Li, Z.; Yi, L.; Liu, F. Comparative study on combustion and emissions between methanol port-injection engine and methanol direct-injection engine with H₂-enriched port-injection under lean-burn conditions. *Energy Convers. Manag.* **2019**, *200*, 112096. [\[CrossRef\]](#)
10. Gong, C.; Peng, L.; Chen, Y.; Liu, J.; Liu, F.; Han, Y. Computational study of intake temperature effects on mixture formation, combustion and unregulated emissions of a DISI methanol engine during cold start. *Fuel* **2018**, *234*, 1269–1277. [\[CrossRef\]](#)
11. Jamrozik, A. The effect of the alcohol content in the fuel mixture on the performance and emissions of a direct injection diesel engine fueled with diesel–methanol and diesel–ethanol blends. *Energy Convers. Manag.* **2017**, *148*, 461–476. [\[CrossRef\]](#)
12. Sayin, C.; İlhan, M.; Canakci, M.; Gumus, M. Effect of injection timing on the exhaust emissions of a diesel engine using diesel–methanol blends. *Renew. Energy* **2009**, *34*, 1261–1269. [\[CrossRef\]](#)
13. Zhang, Z.; Tian, J.; Xie, G.; Li, J.; Xu, W.; Jiang, F.; Huang, Y.; Tan, D. Investigation on the combustion and emission characteristics of diesel engine fueled with diesel/methanol/n-butanol blends. *Fuel* **2022**, *314*, 123088. [\[CrossRef\]](#)
14. Li, Z.; Wang, Y.; Geng, H.; Zhen, X.; Liu, M.; Xu, S.; Li, C. Parametric study of a diesel engine fueled with directly injected methanol and pilot diesel. *Fuel* **2019**, *256*, 115882. [\[CrossRef\]](#)
15. Di Iorio, S.; Catapano, F.; Magno, A.; Sementa, P.; Vaglieco, B.M. The Potential of Ethanol/Methanol Blends as Renewable Fuels for DI SI Engines. *Energies* **2023**, *16*, 2791. [\[CrossRef\]](#)
16. Ma, B.; Yao, A.; Yao, C.; Wu, T.; Wang, B.; Gao, J.; Chen, C. Exergy loss analysis on diesel methanol dual fuel engine under different operating parameters. *Appl. Energy* **2020**, *261*, 114483. [\[CrossRef\]](#)
17. Geng, P.; Yao, C.; Wei, L.; Liu, J.; Wang, Q.; Pan, W.; Wang, J. Reduction of PM emissions from a heavy-duty diesel engine with diesel/methanol dual fuel. *Fuel* **2014**, *123*, 1–11. [\[CrossRef\]](#)
18. Liu, J.; Yao, A.; Yao, C. Effects of diesel injection pressure on the performance and emissions of a HD common-rail diesel engine fueled with diesel/methanol dual fuel. *Fuel* **2015**, *140*, 192–200. [\[CrossRef\]](#)
19. Yao, C.; Cheung, C.S.; Cheng, C.; Wang, Y. Reduction of Smoke and NO_x from Diesel Engines Using a Diesel/Methanol Compound Combustion System. *Energy Fuels* **2007**, *21*, 686–691. [\[CrossRef\]](#)

20. Yao, C.; Cheung, C.S.; Cheng, C.; Wang, Y.; Chan, T.L.; Lee, S.C. Effect of Diesel/methanol compound combustion on Diesel engine combustion and emissions. *Energy Convers. Manag.* **2008**, *49*, 1696–1704. [\[CrossRef\]](#)
21. Xu, C.; Zhuang, Y.; Qian, Y.; Cho, H. Effect on the performance and emissions of methanol/diesel dual-fuel engine with different methanol injection positions. *Fuel* **2022**, *307*, 121868. [\[CrossRef\]](#)
22. Kumar, D.; Valera, H.; Gautam, A.; Agarwal, A.K. Simulations of methanol fueled locomotive engine using high pressure co-axial direct injection system. *Fuel* **2021**, *295*, 120231. [\[CrossRef\]](#)
23. Wang, Y.; Wang, H.; Meng, X.; Tian, J.; Wang, Y.; Long, W.; Li, S. Combustion characteristics of high pressure direct-injected methanol ignited by diesel in a constant volume combustion chamber. *Fuel* **2019**, *254*, 115598. [\[CrossRef\]](#)
24. Ning, L.; Duan, Q.; Kou, H.; Zeng, K. Parametric study on effects of methanol injection timing and methanol substitution percentage on combustion and emissions of methanol/diesel dual-fuel direct injection engine at full load. *Fuel* **2020**, *279*, 118424. [\[CrossRef\]](#)
25. Jia, Z.; Denbratt, I. Experimental investigation into the combustion characteristics of a methanol-Diesel heavy duty engine operated in RCCI mode. *Fuel* **2018**, *226*, 745–753. [\[CrossRef\]](#)
26. Li, Z.; Wang, Y.; Yin, Z.; Gao, Z.; Wang, Y.; Zhen, X. To achieve high methanol substitution ratio and clean combustion on a diesel/methanol dual fuel engine: A comparison of diesel methanol compound combustion (DMCC) and direct dual fuel stratification (DDFS) strategies. *Fuel* **2021**, *304*, 121466. [\[CrossRef\]](#)
27. Li, Z.; Wang, Y.; Yin, Z.; Gao, Z.; Wang, Y.; Zhen, X. An exploratory numerical study of a diesel/methanol dual-fuel injector: Effects of nozzle number, nozzle diameter and spray spacial angle on a diesel/methanol dual-fuel direct injection engine. *Fuel* **2022**, *318*, 123700. [\[CrossRef\]](#)
28. Li, Z.Y.; Wang, Y.; Yin, Z.B.; Geng, H.M.; Zhu, R.; Zhen, X.D. Effect of injection strategy on a diesel/methanol dual-fuel direct-injection engine. *Appl. Therm. Eng.* **2021**, *189*, 116691. [\[CrossRef\]](#)
29. Han, D.; Wang, Q.; He, Z.; Tan, X.; Shao, C.; Jin, Y. Influence of the Position of Nozzle Holes on Combustion and Emissions for a Direct Injection Dual Fuel Engine. *Trans. CSICE* **2017**, *35*, 238–245.
30. Doppalapudi, A.T.; Azad, A.K.; Khan, M.M.K. Analysis of Improved In-Cylinder Combustion Characteristics with Chamber Modifications of the Diesel Engine. *Energies* **2023**, *16*, 2586. [\[CrossRef\]](#)
31. Sarathy, S.M.; Oßwald, P.; Hansen, N.; Kohse-Höinghaus, K. Alcohol combustion chemistry. *Progr. Energy Combust. Sci.* **2014**, *44*, 40–102. [\[CrossRef\]](#)
32. Chang, Y.; Jia, M.; Li, Y.; Xie, M. Application of the Optimized Decoupling Methodology for the Construction of a Skeletal Primary Reference Fuel Mechanism Focusing on Engine-Relevant Conditions. *Front. Mech. Eng.* **2015**, *1*, 11. [\[CrossRef\]](#)
33. Han, Z.; Reitz, R.D. Turbulence Modeling of Internal Combustion Engines Using RNG κ - ϵ Models. *Combust. Sci. Technol.* **1995**, *106*, 267–295. [\[CrossRef\]](#)
34. O'Rourke, P.J.; Amsden, A.A. A Spray/Wall Interaction Submodel for the KIVA-3 Wall Film Model. *SAE Trans.* **2000**, *109*, 281–298.
35. Ricart, L.M.; Reitz, R.D.; Dec, J.E. Comparisons of Diesel Spray Liquid Penetration and Vapor Fuel Distributions With In-Cylinder Optical Measurements. *J. Eng. Gas Turbines Power.* **1999**, *122*, 588–595. [\[CrossRef\]](#)
36. Han, Z.; Reitz, R.D. A temperature wall function formulation for variable-density turbulent flows with application to engine convective heat transfer modeling. *Int. J. Heat Mass Transfer.* **1997**, *40*, 613–625. [\[CrossRef\]](#)
37. Schmidt, D.P.; Rutland, C.J. A new droplet collision algorithm. *J. Comput. Phys.* **2000**, *164*, 62–80. [\[CrossRef\]](#)
38. Senecal, P.K.; Pomraning, E.; Richards, K.J.; Briggs, T.E.; Choi, C.Y.; McDavid, R.M.; Patterson, M.A. Multi-Dimensional Modeling of Direct-Injection Diesel Spray Liquid Length and Flame Lift-off Length using CFD and Parallel Detailed Chemistry. In Proceedings of the SAE World Congress & Exhibition, Detroit, MI, USA, 3–6 March 2003.
39. Li, Z.; Wang, Y.; Yin, Z.; Gao, Z.; Wang, Y.; Zhen, X. Parametric study of a single-channel diesel/methanol dual-fuel injector on a diesel engine fueled with directly injected methanol and pilot diesel. *Fuel* **2021**, *302*, 121156. [\[CrossRef\]](#)
40. Maroteaux, F.; Saad, C. Combined mean value engine model and crank angle resolved in-cylinder modeling with NO_x emissions model for real-time Diesel engine simulations at high engine speed. *Energy* **2015**, *88*, 515–527. [\[CrossRef\]](#)
41. Zang, R.; Yao, C. Numerical Study of Combustion and Emission Characteristics of a Diesel/Methanol Dual Fuel (DMDF) Engine. *Energy Fuels* **2015**, *29*, 3963–3971. [\[CrossRef\]](#)
42. Zhen, X.; Ming, J.; Xu, G.; Li, Y.; Lu, X. Potential for reducing emissions in reactivity controlled compression ignition (RCCI) engine by fueling syngas and diesel. *Energy Fuels* **2018**, *32*, 3869–3882.
43. Li, Y.; Jia, M.; Liu, Y.; Xie, M. Numerical study on the combustion and emission characteristics of a methanol/diesel reactivity controlled compression ignition (RCCI) engine. *Appl. Energy* **2013**, *106*, 184–197. [\[CrossRef\]](#)
44. Cengiz, C.; Unverdi, S.O. A CFD Study on the Effects of Injection Timing and Spray Inclusion Angle on Performance and Emission Characteristics of a DI Diesel Engine Operating in Diffusion-Controlled and PCCI Modes of Combustion. *Energies* **2023**, *16*, 2861. [\[CrossRef\]](#)
45. Xu, C.; Cho, H. Effect of Methanol/Water Mixed Fuel Compound Injection on Engine Combustion and Emissions. *Energies* **2021**, *14*, 4491. [\[CrossRef\]](#)
46. Dwarshala, S.K.R.; Rajakumar, S.S.; Kummitha, O.R.; Venkatesan, E.P.; Veza, I.; Samuel, O.D. A Review on Recent Developments of RCCI Engines Operated with Alternative Fuels. *Energies* **2023**, *16*, 3192. [\[CrossRef\]](#)
47. Xu, H.; Yao, C.; Xu, G. Chemical kinetic mechanism and a skeletal model for oxidation of n-heptane/methanol fuel blends. *Fuel* **2012**, *93*, 625–631. [\[CrossRef\]](#)

Disclaimer/Publisher’s Note: The statements, opinions and data contained in all publications are solely those of the individual author(s) and contributor(s) and not of MDPI and/or the editor(s). MDPI and/or the editor(s) disclaim responsibility for any injury to people or property resulting from any ideas, methods, instructions or products referred to in the content.